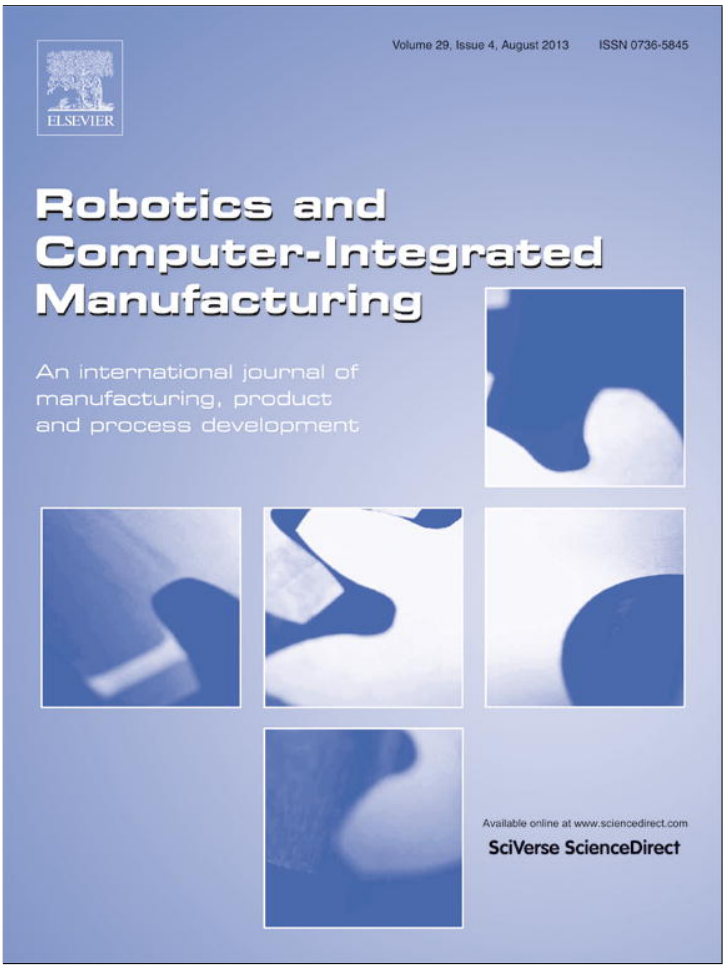

Robotics and Computer-Integrated Manufacturing 29 (2013) 158–173

Contents lists available at SciVerse ScienceDirect

Robotics and Computer-Integrated Manufacturing

journal homepage: www.elsevier.com/locate/rcim

Position, Jacobian and workspace analysis of a 3-PSP spatial parallel manipulator

Amir Rezaei [a,*], Alireza Akbarzadeh [a], Payam Mahmoodi Nia [a], Mohammad-R. Akbarzadeh-T [b]

[a] Mechanical Engineering Department, Center of Excellence on Soft Computing and Intelligent Information Processing, (SCIIP), Ferdowsi University of Mashhad, Mashhad, Iran
[b] Electrical Engineering Department, Center of Excellence on Soft Computing and Intelligent Information Processing, (SCIIP), Ferdowsi University of Mashhad, Mashhad, Iran

ARTICLE INFO

Article history:
Received 25 April 2012
Received in revised form
12 October 2012
Accepted 29 November 2012
Available online 16 January 2013

Keywords:
Spatial parallel manipulator
Kinematics
Jacobian analysis
Singularity
Workspace

ABSTRACT

This paper investigates the problems of kinematics, Jacobian, singularity and workspace analysis of a spatial type of 3-PSP parallel manipulator. First, structure and motion variables of the robot are addressed. Two operational modes, non-pure translational and coupled mixed-type are considered. Two inverse kinematics solutions, an analytical and a numerical, for the two operational modes are presented. The direct kinematics of the robot is also solved utilizing a new geometrical approach. It is shown, unlike most parallel robots, the direct kinematics problem of this robot has a unique solution. Next, analytical expressions for the velocity and acceleration relations are derived in invariant form. Auxiliary vectors are introduced to eliminate passive velocity and acceleration vectors. The three types of conventional singularities are analyzed. The notion of non-pure rotational and non-pure translational Jacobian matrices is introduced. The non-pure rotational and non-pure translational Jacobian matrices are combined to form the Jacobian of constraint matrix which is then used to obtain the constraint singularity. Finally, two methods, a discretization method and one based on direct kinematics are presented and robot non-pure translation and coupled mixed-type reachable workspaces are obtained. The influence of tool length on workspace is also studied.

1. Introduction

Parallel kinematic machines (PKMs) have shown to offer many advantages such as, high positioning accuracy, high static/dynamic inherent rigidity, low inertia, high nominal load-to-weight ratio and good dynamic performance. However, the principal drawbacks of the PKMs are small and complex workspace, commonly coupled position and orientation of moving platform as well as difficult forward position kinematics [1–3].

Earlier PKMs were designed mostly with 6 degrees of freedom (DOFs). However, there are many practical applications where 6-DOFs are not all required [4]. The PKMs with the lower DOFs have most of the inherent capabilities of the parallel robots and can be made with lower manufacturing cost [3,5]. However, some spatial PKMs with lower DOFs present application complications due to the commonly coupled position and orientation of the moving platform. The 3-DOF PKMs can be classified into three categories with respect to the type of DOF used by their moving platform. These categories are: (a) translational, (b) rotational and (c) coupled mixed-types motion (two translational and one rotational, T2R1-type, or two rotational and one translational, R2T1-type). The motions in each of these categories may be pure or non-pure. Many literatures have studied the famous pure translational robots such as the 3-UPU [6], the CUR [7] and the 3-PRC [8]. There is extensive research work focused on the famous DELTA robot with three translational DOFs [9]. Also, many studies are completed on pure rotational PKMs such as spherical robots [10,11] and the Agile Eye mechanism [12]. The PKMs with coupled mixed-types of motions are also studied, for example, the 3-PRS [1] and the CaPaMan [13]. In addition Li and Hervé [14] studies a number of pure R2T1 type parallel robots.

In this paper, a specific architecture of the 3-PSP fully parallel robot is selected and its position, Jacobian and workspace analysis are investigated. The 3-PSP robot is a spatial 3-DOF parallel robot with symmetric geometry and three identical PSP legs (Prismatic–Spherical–Prismatic). The 3-PSP robot offers the advantage of allowing the user to select its desired DOFs. The user may select to run the robot either in non-pure translational or coupled mixed-type modes. This feature potentially allows use of different applications for the 3-PSP robot.

Unlike their serial counterparts, the inverse kinematics problem of PKMs is often simpler to solve than its direct kinematics problem. However, obtaining analytical solution to direct and inverse kinematics of 3-PSP are both difficult. The difficulty in

* Corresponding author.
E-mail addresses: amirrezaei_aico@yahoo.com (A. Rezaei), ali_akbarzadeh_t@yahoo.com (A. Akbarzadeh), p.mahmoodinia@gmail.com (P.M. Nia). akbarzadeh@ieee.org (M.-R. Akbarzadeh-T).

0736-5845/$ - see front matter © 2012 Elsevier Ltd. All rights reserved.
http://dx.doi.org/10.1016/j.rcim.2012.11.009

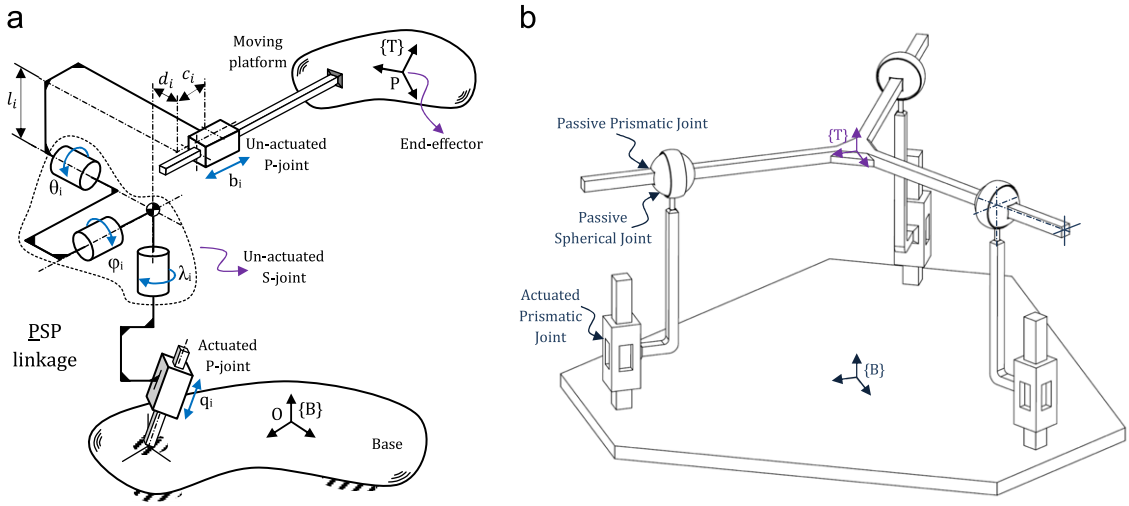

Fig. 1. (a) A kinematic chain of a general 3-PSP parallel robot and (b) a simplified equivalent form of the spatial 3-PSP parallel manipulator

solving the inverse kinematics of the 3-PSP robot depends on the DOFs selected for the moving platform [15–17]. The direct kinematics of PKMs commonly involve the solution for a system of nonlinear coupled algebraic equations in the variables describing pose parameters of the moving platform [6]. To solve direct kinematics problem, either numerical or analytical approaches are used. However, usually, finding the exact analytical solutions is difficult [6]. Kamali and Akbarzadeh [18] presented a method for a general solution to the direct kinematics problem of non-cuspidal parallel manipulators in trajectory following by introducing a new concept based on basic regions. In a thesis presented by Bonev [19], the effectiveness of geometric methods to design and analyze parallel mechanisms is presented. He presented a brief discussion on the 3-PSP and obtained its kinematics constraint equations leading to motion equations for the center of the platform. Di Gregorio solved the position analysis of a general 3-PSP parallel robot in analytical form [16]. To solve the direct position analysis, an algebraic system which has a Sylvester eliminant that is a polynomial equation of the 8th degree in one of the unknowns is obtained. In the present paper, the direct kinematics of the 3-PSP robot is solved utilizing a new geometrical approach. We also show that the direct kinematics problem of this robot, unlike most parallel robots, has only one unique real answer.

To define and evaluate the performances of a manipulator, Jacobian and singularity analyses are commonly used [20,21]. These analyses have been studied by many literatures [21–23]. Firmani and Podhorodeski [24] described singularity of planar parallel manipulators based on forward kinematic solutions. Also, Enferadi and Akbarzadeh [10] studied singularity of a novel spherical parallel manipulator using obtained Jacobian matrices from position equations. The workspace of the PKMs has also been extensively studied using different methods [25–27]. Examples of common 3-DOF workspaces include reachable, maximal and dexterous workspace [20]. To the best of authors' knowledge, the Jacobian, singularity and workspace analysis are not previously reported for the 3-PSP robot.

This paper is organized as follows. In Sections 2 and 3, structure and motion variables of the robot are addressed and two separate operational modes, coupled mixed-type and non-pure translational, are presented, respectively. In Section 4, inverse kinematics is discussed. A numerical method for the coupled mixed-type mode and an analytical method for the non-pure translational mode are presented. In Section 5, the direct kinematics of the robot is solved utilizing a new geometrical approach. In Section 6, using vector analysis, analytical expressions for velocity and acceleration relations are derived in invariant form. Additionally, we introduce the non-pure rotational and non-pure translational Jacobian matrices and use them to derive the relationship between angular and translational velocities of the moving platform and the actuated joint rates. Using non-pure rotational and non-pure translational Jacobian matrices, Jacobian of constraint is defined. In Section 7, using Jacobian matrices, obtained in analytical form, the three conventional types of singularities are analyzed. Furthermore, using Jacobian of constraint matrix, the constraint singularity is obtained for the 3-PSP robot. Finally, in Section 8, two numerical methods are presented and used to calculate the robot non-pure translation and coupled mixed-type reachable workspaces. Influence of the tool length on non-pure translation workspace is also studied. Concluding remarks are made in last section of the paper.

2. Structural description of a spatial 3-PSP parallel robot

In this paper, a special type of a 3-PSP parallel robot with specific architecture is investigated. The spatial 3-PSP robot is fully parallel with three DOFs in space. The robot is composed of a moving platform which is shaped like a symmetric tripetalous star, called moving star (MS), and two fixed platforms. The MS is formed by three branches, forming a planar star with each branch making an angle of $\gamma=120^\circ$ with the other. Various tools, end-effectors, may be placed in the center of the MS. The MS and the fixed platforms are connected together using three parallel legs with identical serial kinematic chains. Each of the three legs, consists of an active prismatic joint (P-joint) which is actuated by a Linear rod (LR), a passive spherical joint (S-joint) and a passive prismatic joint (P-joint). The MS is attached to the base by three identical serial PSP linkages. The three closed kinematics loops make the 3-PSP parallel manipulator. The actuation system for each leg is made of a motor, a gear box and a ball screw assembly. A kinematic chain of a general 3-PSP parallel robot is shown in Fig. 1(a). A simplified equivalent form of the spatial 3-PSP parallel manipulator investigated in this paper is shown in Fig. 1(b). Note that for the spatial 3-PSP, parameters l_i, c_i and d_i shown in Fig. 1(a) are all set to zero which insures the axis of the passive prismatic and spherical joints intersect.

The solid and physical models of a 3-PSP parallel manipulator are also illustrated in Fig. 2.

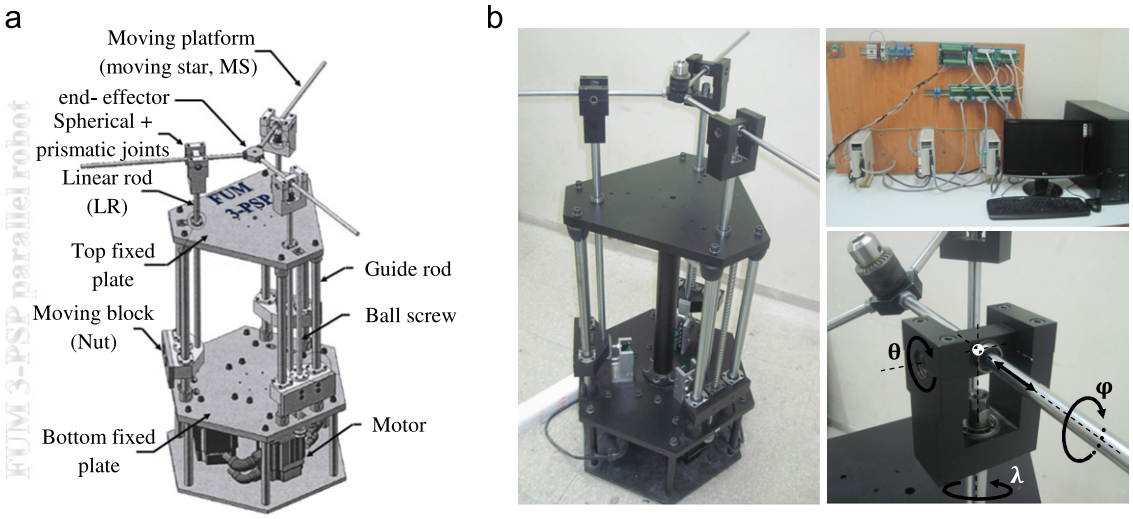

Fig. 2. The 3-PSP parallel manipulator: (a) solid model and (b) physical model and its controller.

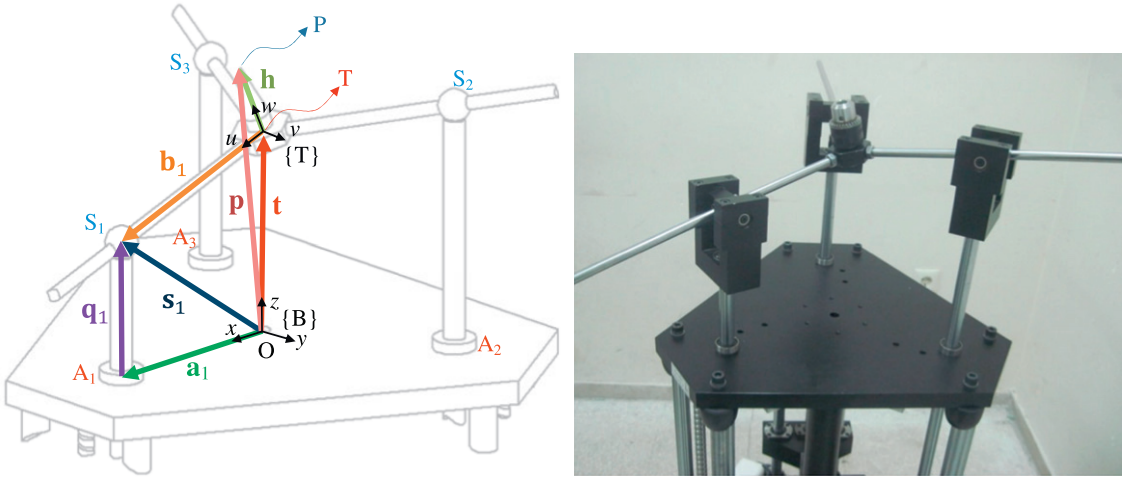

Fig. 3. The vectors and coordinate frames for one typical kinematic chain of the 3-PSP parallel robot.

3. Description of vectors, reference frames, motion variables and DOFs

Fig. 3 represents vectors and coordinate frames used for the inverse kinematics problem of the 3-PSP. For this purpose, a fixed coordinate frame $B\{x,y,z\}$ is embedded in the top fixed platform, at center point O of fixed triangle $\Delta A_1A_2A_3$. Likewise a moving coordinate frame $T\{u,v,w\}$ is attached to the tool, at point T. Point P defines the position of the tool tip and is located along the z-axis of frame $\{T\}$. In this paper, a leading superscript represents the coordinate frame in which the vector is referenced. Additionally, bold lower and upper case lettering designate vectors and matrices, respectively. The three spherical joints are denoted byS_i (for$i=1$, 2 and 3) and their positions with respect to point O are denoted by ${}^B\mathbf{s}_i$. Three position vectors ${}^B\mathbf{q}_i$ specify length of each linear rod (LR) and connect corners of the fixed triangle, A_i, to the center of the spherical joints, S_i. Position of the end-effector, point T, and tool tip, point P, with respect to $\{B\}$ is given by vector ${}^B\boldsymbol{t}=[x_T,y_T,z_T]^T$ and ${}^B\mathbf{p}=[x_P,y_P,z_P]^T$, respectively. Three additional position vectors, ${}^B\mathbf{a}_i$ locate corners of the fixed base, A_i, in $\{B\}$. Further, the position vector ${}^T\mathbf{h}$, defined in $\{T\}$, is a vector which connects point T to point P. The length of this vector, $\mathbf{h}$, defines the length of the tool. Finally, the position vector ${}^T\mathbf{b}_i$, connects the end-effector, point T, to the ith spherical joint, S_i.

Assume the 3-PSP consists of "r" movable rigid bodies which are connected together by "m" one-DOF joints. A multi-DOF joint like a spherical joint can be considered as three one-DOF revolute joints linked with two movable rigid bodies having zero mass and dimension. Therefore, the DOF of the 3-PSP can be calculated using the Chebyshev–Grübler–Kutzbach formula as

$$\mathrm{DOF}=6r-5m=6\times 13-5\times 15=3 \tag{1}$$

As shown in Eq. (1), the 3-PSP parallel robot has 3-DOFs in space. We know that, the degrees of freedom for parallel robots are equal to the number of independent motion variables for the moving platform. Therefore, only three DOFs of the total six DOFs considered for the MS are independent and are so-called controllable. The desired motion variables of the MS, may be selected as

Selection #1—Operational Mode $\theta\varphi Z$: Two rotational DOFs about x- and y-axis, θ and φ, and one translational DOF along z-axis.
Selection #2—Operational Mode XYZ : Three non-pure translational DOFs along x, y and z-axis.

Therefore, when solving the inverse kinematics problem and performing workspace analysis, depending on the selected DOFs, two separate solution strategies are considered. These strategies

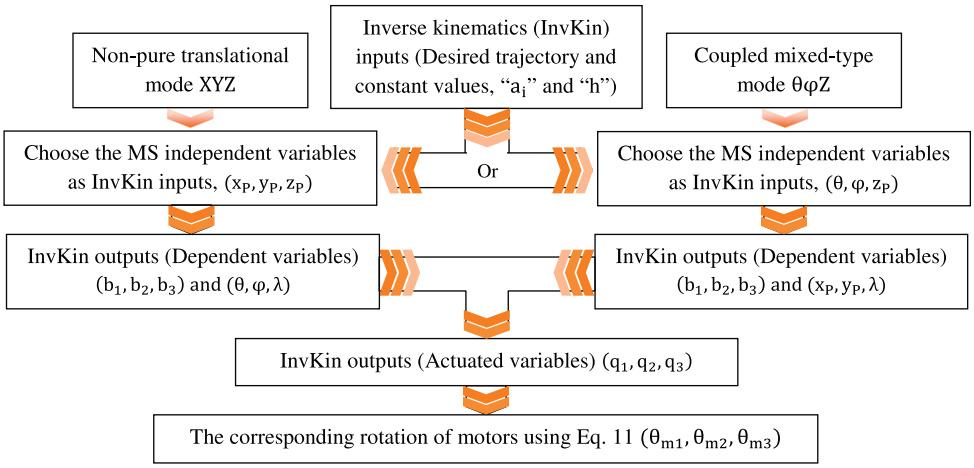

Fig. 4. Inverse kinematics process diagram for the 3-PSP parallel manipulator.

will be explained in the next section. The following variables are used.

- *Variables used for MS*

Rotational variables about the x-, y- and z-axis (Euler angles): θ, φ, λ
Translational variables of the MS center, point T, along the x-, y- and z-axis: x_T, y_T, z_T
Translational variables for the tool tip, point T, along the x, y and z-axis: x_P, y_P, z_P

- *Variables used for linear motion of the linear rods*

Translational variables for the linear rods, LRs: q_1, q_2,q_3

- *Variables used for linear motion of the MS branches*

Translational variables for the MS branches: b_1,b_2,b_3

Therefore, depending on the selected DOFs, three of the six MS variables are chosen and the remaining nine variables are calculated using inverse kinematics problem. The inverse kinematics solution process for the two operational modes is illustrated in Fig. 4.

4. Inverse position analysis

To perform analyses such as Jacobian analysis, dynamics, trajectory planning and stiffness analysis, we need to have the robot kinematic variables [28,29]. Consider Fig. 3. The position vectors used to describe the kinematic configuration of the 3-PSP parallel manipulator can be expressed by

$$ {}^B\mathbf{a}_1 = [a \quad 0 \quad 0]^T, \quad {}^B\mathbf{a}_2 = [-\tfrac{1}{2}a \quad \tfrac{\sqrt{3}}{2}a \quad 0]^T, $$
$$ {}^B\mathbf{a}_3 = [-\tfrac{1}{2}a \quad -\tfrac{\sqrt{3}}{2}a \quad 0]^T \tag{2} $$

$$ {}^T\mathbf{b}_1 = [b_1 \quad 0 \quad 0]^T, \quad {}^T\mathbf{b}_2 = [-\tfrac{1}{2}b_2 \quad \tfrac{\sqrt{3}}{2}b_2 \quad 0]^T, $$
$$ {}^T\mathbf{b}_3 = [-\tfrac{1}{2}b_2 \quad -\tfrac{\sqrt{3}}{2}b_2 \quad 0]^T \tag{3} $$

$$ {}^B\mathbf{q}_i = [0 \quad 0 \quad q_i]^T \text{ for } i = 1,2,3 \tag{4} $$

$$ {}^B\mathbf{t} = [x_T \quad y_T \quad z_T]^T, \quad {}^B\mathbf{p} = [x_P \quad y_P \quad z_P]^T, \quad {}^B\mathbf{h} = [0 \quad 0 \quad h]^T \tag{5} $$

To transfer a vector defined in $\{T\}$ to $\{B\}$, we can use a rotation matrix, ${}^B_T\mathbf{R}$, which consists of three Euler angles θ, ϕ and λ about x, y and z-axis of the fixed reference frame $\{B\}$. For this purpose, three unit vectors $\mathbf{u}$, $\mathbf{v}$ and $\mathbf{w}$ along the u-, v- and w-axis of the moving coordinate frame $\{T\}$ are defined. Therefore, the rotation matrix, ${}^B_T\mathbf{R}$, using these unit vectors is

$$ {}^B_T\mathbf{R} = \mathbf{R}_{z,\lambda}\mathbf{R}_{y,\varphi}\mathbf{R}_{x,\theta} = \begin{bmatrix} u_x & v_x & w_x \\ u_y & v_y & w_y \\ u_z & v_z & w_z \end{bmatrix} $$
$$ = \begin{bmatrix} c\lambda c\varphi & -s\lambda c\theta + c\lambda\, \varphi s\theta & s\lambda s\theta + c\lambda s\varphi c\theta \\ s\lambda c\varphi & c\lambda c\theta + s\lambda s\varphi s\theta & -c\lambda s\theta + s\lambda s\varphi c\theta \\ -s\varphi & c\varphi s\theta & c\varphi c\theta \end{bmatrix} \tag{6} $$

where c and s stand for cosine and sine, respectively. Therefore, the position vector ${}^B\mathbf{b}_i$, in $\{B\}$, which connects the end-effector, point T, to the ith spherical joint, S_i, can be expressed as

$$ {}^B\mathbf{b}_i = {}^B_T\mathbf{R}\,{}^T\mathbf{b}_i \quad \text{for } i = 1,2,3 \tag{7} $$

Considering Fig. 3, we can write

$$ {}^B\mathbf{t} = {}^B\mathbf{p} - {}^B\mathbf{h}, \quad {}^B\mathbf{h} = {}^B_T\mathbf{R}\,{}^T\mathbf{h} \tag{8} $$

For each kinematics chain, we can write a closed loop vector equation as

$$ {}^B\mathbf{a}_i + {}^B\mathbf{q}_i = {}^B\mathbf{b}_i + {}^B\mathbf{t} \quad \text{for } i = 1,2,3 \tag{9} $$

Substituting Eqs. (7) and (8) into Eq. (9), yields

$$ {}^B\mathbf{a}_i + {}^B\mathbf{q}_i = {}^B_T\mathbf{R}({}^T\mathbf{b}_i - {}^T\mathbf{h}) + {}^B\mathbf{p} \quad \text{for } i = 1,2,3 \tag{10} $$

The vector equations, Eq. (10), are called kinematics constraint equations. These equations consist of three vector equations and are equal to a set of nine non-linear scalar equations. In inverse kinematics, InvKin, problem, three chosen independent variables for the MS are given. Next, values for lengths of the LRs, q_i, and subsequently the corresponding values for rotational position of motors, θ_{mi}, are determined. As shown in Fig. 5, we can represent the relationship between the linear displacement of nuts and corresponding rotational displacement of motors as

$$ \theta_{mi} = \left(\frac{N\pi}{l_b}\right) q_i \tag{11} $$

where l_b and N are the lead of the ball screws and gearbox transmission ratio, respectively.

4.1. The first operational mode, coupled mixed-type mode $\theta\varphi Z$

In this problem, the orientation of the MS about x- and y-axis of the frame $\{B\}$ and translation of the tool along z-axis are considered as inputs of the InvKin problem. In this mode, the three motion variables x, y and λ are dependent on the remaining

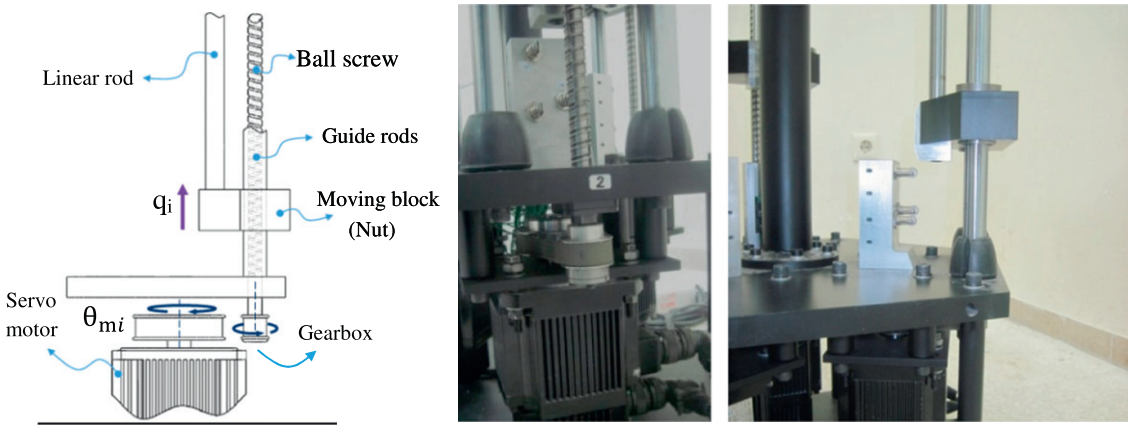

Fig. 5. The *i*th motor, ball screw and nut assembly.

motion variables θ, ϕ and z. Typical applications of this mode include orienting a laser device as well as simulator platforms. It is also possible to install the 3-PSP robot on an *XY* table and achieve a hybrid robot with 5 independent DOFs. In this case, the hybrid robot may be used as a 5-axis CNC machine head.

4.1.1. Numerical solution for inverse kinematics problem

When variables (θ,ϕ,z_P) are chosen as inputs, finding the analytical solution for Eq. (10) is rather difficult. Therefore, a numerical approach may be employed to find a local solution. In this paper, a set of 9 nonlinear algebraic equations, shown in Appendix A, are extracted from Eq. (10). These nine equations are numerically solved using Newton iterative method as

Algorithm: Numerical solution for inverse kinematics problem using Newton's method

1. Constant inputs: a and h
2. Inputs: Trajectory$=[z_P, \theta, \varphi]_{n\times 3}$, n=number of discrete data points on the trajectory
3. Error$=10^{-6}$ (m) An arbitrary small value (Tolerance)
4. Find an initial guess as a 9×1 vector $\mathbf{x}_0=[\mathbf{q}_i,\mathbf{b}_i,x_P,y_P,\lambda]_{1\times 9}$ for $i=1,2,3$

For $j=1$: n

While$||\psi(\mathbf{x}_j)|| >$ error

$\mathbf{x}_j=\mathbf{x}_{j-1}-(\frac{\partial\psi(\mathbf{x}_{j-1})}{\partial\mathbf{x}})^{-1}\psi(\mathbf{x}_{j-1})$

End while

If $0\le\mathbf{x}_j(1)=q_1\le 0.4$ m and $0\le\mathbf{x}_j(2)=q_2\le 0.4$ m and $0\le\mathbf{x}_j(3)=q_3\le 0.4$ m

$\mathbf{x}_{j-1}=\mathbf{x}_j$ Update the initial guess for next level and save $\mathbf{x}_{j1\times 9}$

else, $\mathbf{x}_j$ is not a correct answer (is not within the bounds of ball screw travel)

Next n

$\mathbf{x}_{j1\times 9}$ is the answer to the inverse kinematics problem for the jth point of the trajectory.

The proposed Newton's method is not computationally efficient and may not be used for real time control. Additionally, in most robotics applications the inverse kinematics is solved offline. Therefore, its efficiency is not that critical. Yet, various researchers have presented methods to improve the computation time [6,30].

Next, two cases for the InvKin problem are considered and the Newton's method is used to obtain the solutions. In the first case, the length of the tool is assumed to be zero while the second case assumes tool length of $h=8$ cm. Results are depicted in Fig. 6 and Table 1. To provide a better visual perspective, the tool position at $\theta=0$, $\varphi=0$ and $z_T=0.25$ m are also shown in this figure.

4.2. The second operational mode, non-pure translational mode XYZ

In this problem, the Cartesian position of the tool tip with respect to the *x*-, *y*- and *z*-axis of the frame $\{B\}$ are used as inputs and corresponding lengths of the LRs, q_i, are considered as outputs of the InvKin problem. In this mode, the three motion variables θ, ϕ and λ are dependent on the remaining motion variables *x*, *y* and *z*. In author's opinion, this mode does not have much practical applications. This is because in addition to having non-pure motion, small motions in *x*, *y* and *z* may require large changes in θ, ϕ and λ. In our laboratory, we have mostly used this mode for teaching applications as path traveled by tool tip can be easily, physically, observed.

4.2.1. Analytical solution for inverse kinematics problem

Consider Fig. 7. Three constraint scalar equations are required to express the relationship between inputs,(x_P,y_P,z_P), and outputs parameters,(q_1,q_2,q_3). According to structure of the robot, we know that the position of the three *S*-joints, S_i, and center of the MS, point *T*, are located on the MS plane. Then, for the first constraint equation, we will use the position of the three *S*-joints and center of the MS to obtain equation of the MS plane.

$$(\hat{\mathbf{s}}_{normal})\cdot(\mathbf{s}_i-\mathbf{t})=0 \tag{12a}$$

The scalar representation of Eq. (12a) may be expressed by

$$A(x-x_T)+B(y-y_T)+C(z-z_T)=0 \tag{12b}$$

where scalar parameters *A*, *B* and *C* are components of the normal unit vector to the MS plane called $\hat{\mathbf{s}}_{normal}$. This unit vector can be defined as

$$\hat{\mathbf{s}}_{normal}=\frac{\mathbf{s}_{12}\times\mathbf{s}_{13}}{\|\mathbf{s}_{12}\times\mathbf{s}_{13}\|}=[A\quad B\quad C]^T \tag{13}$$

where $\mathbf{s}_{12}$ and $\mathbf{s}_{13}$ are position vectors which connect the first *S*-joint, S_1, to the second and third *S*-joints (S_2,S_3), respectively. These vectors are illustrated in Fig. 7 and are define as

$$\mathbf{s}_{ij}=\mathbf{s}_j-\mathbf{s}_i \quad \text{for } i=1,2,3 \text{ and } j=2,3,1 \tag{14}$$

where

$$\mathbf{s}_i=\mathbf{q}_i+\mathbf{a}_i \tag{15}$$

To obtain the second and third constraints, we note that the angles between each two branches of the MS are equal to $\gamma=120^\circ$.

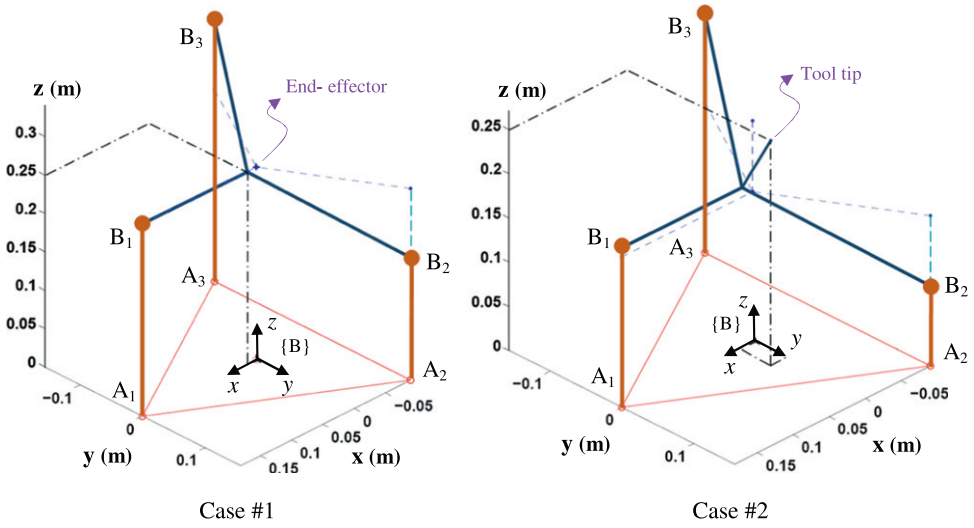

Fig. 6. Inverse kinematics results for mode $\theta\varphi Z$.

Table 1
Inputs/outputs values of InvKin analysis for operational mode θϕZ.

	Inputs			Outputs								
	θ (deg.)	ϕ (deg.)	z_P (m)	q_1 (m)	q_2 (m)	q_3 (m)	x_P (m)	y_P (m)	λ (deg.)	b_1 (m)	b_2 (m)	b_3 (m)
Case #1	−**35.01**	**0**	**0.25**	0.25	0.14	0.36	**0.02**	**0**	0	0.161	0.221	0.221
Case #2	−35.01	0	0.25	0.2645	0.1547	0.3743	0.02	0.046	0	0.161	0.221	0.221

Case #1: a=0.181 m, h=0; Case #2: a=0.181 m, h=0.08 m.

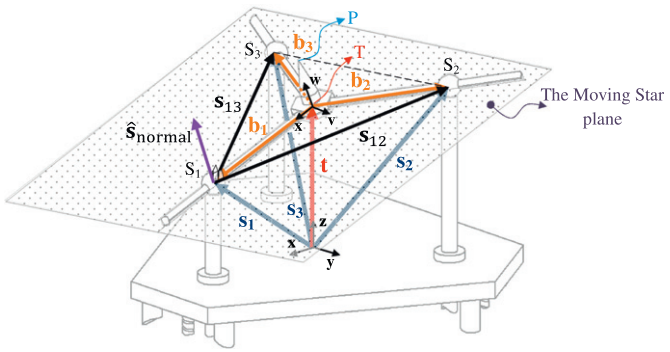

Fig. 7. The MS plane and its related vectors.

Therefore, we can write

$$\mathbf{b}_1.\mathbf{b}_2 = b_1 b_2 \cos(120^\circ), \quad \mathbf{b}_2.\mathbf{b}_3 = b_2 b_3 \cos(120^\circ) \tag{16}$$

Additionally, vectors $\mathbf{b}_i$ can be expressed using center of the MS, point T, and position of the ith S-joint, point S_i, as

$$\mathbf{b}_i = \mathbf{s}_i - \mathbf{t} \tag{17}$$

The magnitude of the vectors, $\mathbf{b}_i$, can be expressed by

$$b_i = \|\mathbf{s}_i - \mathbf{t}\| \tag{18}$$

The three scalar constraint equations required for solving the InvKin problem can be obtained by substituting Eqs. (17) and (18) into Eq. (16), as well as using the MS plane Eq. (12b). These three equations, express relationship between center of the MS position,(x_T,y_T,z_T), and lengths of the LRs, q_i. To obtain the position of the tool tip,(x_P,y_P,z_P), we can use the vector loop Eq. (8).

The vector ${}^B\mathbf{h}$ may be expressed using $\hat{\mathbf{s}}_{normal}$ as

$${}^B\mathbf{h} = h\,\hat{\mathbf{s}}_{normal} \tag{19}$$

Therefore, we can rewrite the vector loop Eq. (8) as

$$\begin{Bmatrix} x_T \\ y_T \\ z_T \end{Bmatrix} = \begin{Bmatrix} x_P \\ y_P \\ z_P \end{Bmatrix} - h \begin{Bmatrix} A \\ B \\ C \end{Bmatrix} \tag{20}$$

Substituting values of the MS center position, Eq. (20), into the three constraint equations as well as substituting any of the S-joints positions into Eq. (12b) will yield three scalar constraint equations based on the position of the tool tip and length of the LRs. Next, MAPLE software may be used to solve the three scalar equations and obtain closed form solution for q_i values as Eq. (21). Note the solutions are values of q_i with respect to the position of the tool tip.

$$q_i = \begin{Bmatrix} f_1(x_P,y_P,z_P,a,h) \\ f_2(x_P,y_P,z_P,a,h) \end{Bmatrix} \text{ for } i = 1,2,3 \tag{21}$$

In this mode of operation, unlike the first, there are two different answers for the InvKin problem of the robot (see Eq. (21)). Once the values of q_i are known, we can obtain corresponding position of the MS center, point T. Therefore, using Eqs. (18) and (20), the values for b_i are obtained. The corresponding Euler angles, using q_i, can be obtained using the rotation matrix, Eq. (6). The rotation matrix, ${}^B_T\mathbf{R}$, is defined using three unit vectors $\mathbf{u}$, $\mathbf{v}$ and $\mathbf{w}$. These unit vectors can be expressed as

$$\mathbf{u} = [\,u_x \quad u_y \quad u_z\,]^T = \frac{\mathbf{b}_1}{\|\mathbf{b}_1\|} \tag{22a}$$

$$\mathbf{w} = [\,w_x \quad w_y \quad w_z\,]^T = \hat{\mathbf{s}}_{normal} \tag{22b}$$

$$\mathbf{v} = [\,v_x \quad v_y \quad v_z\,]^T = \mathbf{w} \times \mathbf{u} \tag{22c}$$

Therefore, the Euler angles using Eqs. (6) and (22) are obtained as

$$\theta = \tan^{-1}\left(\frac{v_z}{w_z}\right), \quad \varphi = \sin^{-1}(-u_z), \quad \lambda = \tan^{-1}\left(\frac{u_y}{u_x}\right) \tag{23}$$

Based on structure of the robot, values greater than 90° are not acceptable. One of the advantages of using the 3-PSP robot in its first mode of operation is that its InvKin problem has a unique solution. However, as will be shown in the workspace section, the *XYZ* mode has a smaller space than the $\theta\phi Z$ mode.

Next, two cases for the InvKin problem are considered. In the first case, the length of the tool is assumed to be zero while the second case assumes tool length of $h=8$ cm. Furthermore, the selected *xyz* input position, is the equal to the output of the $\theta\phi Z$ shown in Table 1—case#1. Results are depicted in Fig. 8 and Table 2.

As expected, by comparing Tables 1 and 2 for the case #1, it can be seen that all related variables are equal. See bold numbers in Tables 1 and 2. Next, InvKin solutions for the case when tool length is non-zero, for the two modes are considered. Results are depicted in Fig. 9 and Table 3. As expected, by observing Table 3, it can be seen that all related variables for one of the solutions are equal (see bold numbers).

5. Direct position analysis

Unlike serial robots, the direct kinematics (DirKin) problem of parallel robots is more involved and complicated. Typically, the DirKin problem of parallel robots leads to solving a high degree polynomial. By solving this equation, several answers are obtained. Some of these answers are in imaginary form and some are physically not reachable by the robot. However, some answers are both real and consistent with physical limitations of the robot structure. These answers are the correct answers. In this section, a new approach for solving the DirKin problem of the 3-PSP is presented. The approach uses the geometry of the robot. We will show that unlike most parallel robots, using the proposed approach, only one answer is obtained for the DirKin problem.

Consider Figs. 3 and 10. The position of three spherical joints, S_i, in the fixed base coordinate frame $\{B\}$ can be determined using $\mathbf{a}_i$ and position of the three moving blocks $\mathbf{q}_i$. The MS plane can

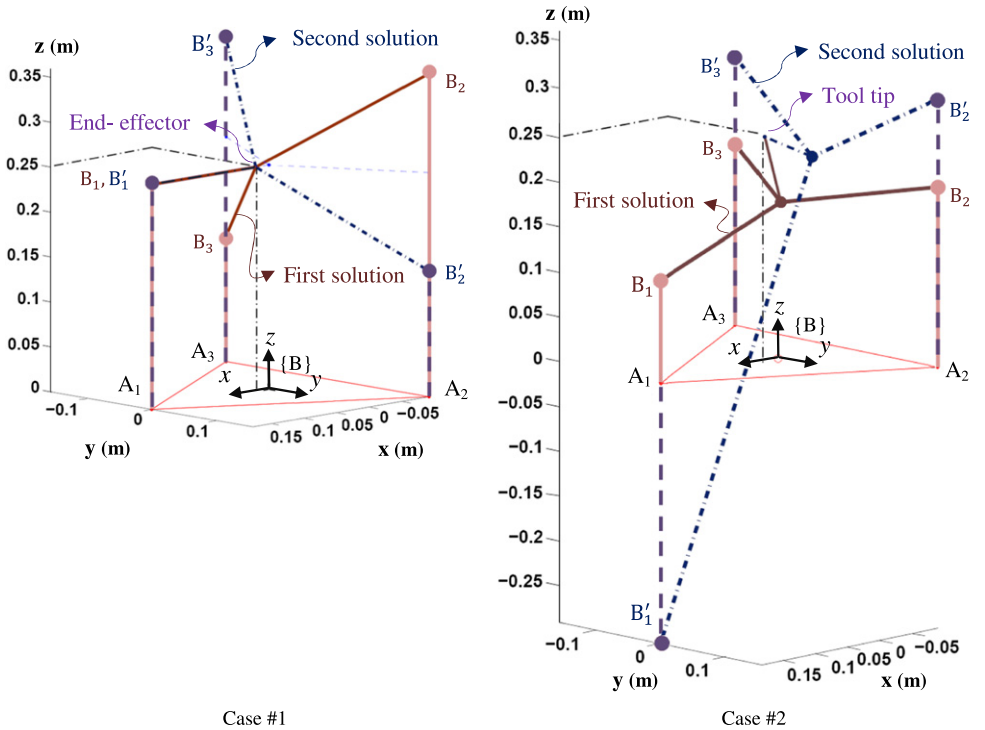

Fig. 8. Inverse kinematics results for mode *XYZ*.

Table 2
Inputs/outputs values of InvKin analysis for operational mode *XYZ*.

	Inputs			Outputs								
	x_p (m)	y_p (m)	z_p (m)	q_1 (m)	q_2 (m)	q_3 (m)	θ (deg.)	φ (deg.)	λ (deg.)	b_1 (m)	b_2 (m)	b_3 (m)
Case #1	**0.02**	**0**	**0.25**	0.25	0.36	0.14	35.01	0	0	0.161	0.221	0.221
				0.25	0.14	0.36	−**35.01**	**0**	0	0.161	0.221	0.221
Case #2	0.02	0	0.25	0.115	0.201	0.201	0	17.65	0	0.194	0.181	0.181
				−0.291	0.299	0.299	0	65.29	0	0.559	0.181	0.181

Case #1: $a=0.181$ m, $h=0$; Case #2: $a=0.181$ m, $h=0.08$ m.

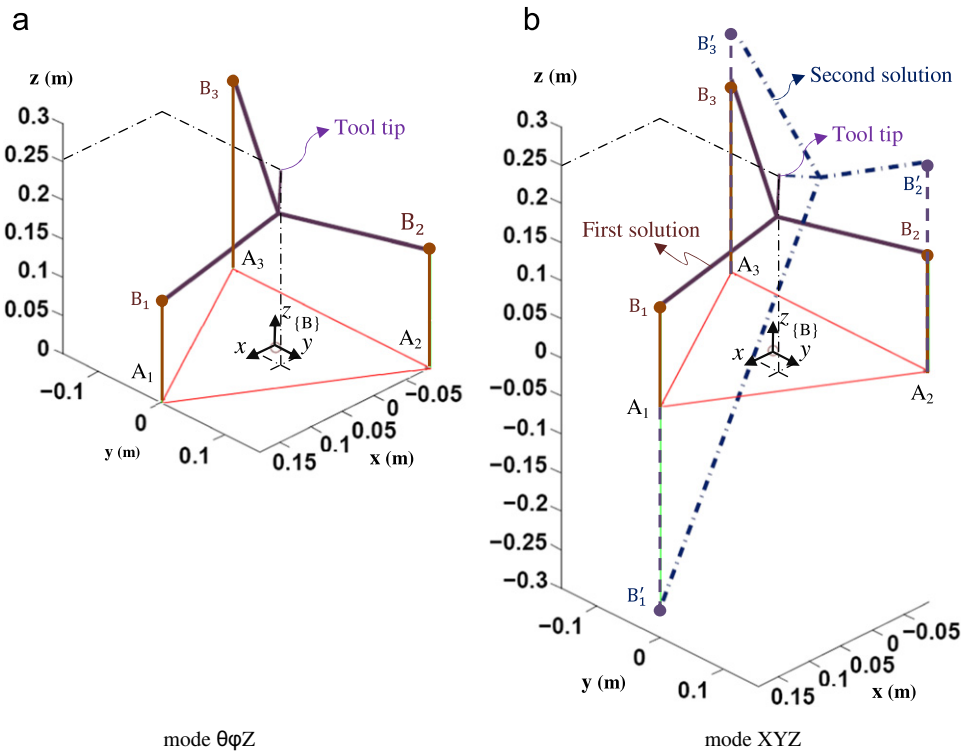

Fig. 9. Comparison between InvKin answers for modes $\theta\varphi Z$ and *XYZ*. (a) mode $\theta\varphi$Z and (b) mode XYZ.

Table 3
Comparison between InvKin answers for modes $\theta\phi Z$ and *XYZ*.

	Inputs			Outputs								
Mode $\theta\phi Z$	θ (deg.)	φ (deg.)	z_P (m)	q_1 (m)	q_2 (m)	q_3 (m)	x_P (m)	y_P (m)	λ (deg.)	b_1 (m)	b_2 (m)	b_3 (m)
	−17.53	**13.54**	**0.25**	0.132	0.152	0.251	**0.02**	**0.03**	−2.09	0.185	0.178	0.202
Mode *XYZ*	x_P (m)	y_P (m)	z_P (m)	q_1 (m)	q_2 (m)	q_3 (m)	θ (deg.)	φ (deg.)	λ (deg.)	b_1 (m)	b_2 (m)	b_3 (m)
	0.02	**0.03**	**0.25**	0.132	0.152	0.251	**−17.53**	**13.54**	−2.09	0.185	0.178	0.202
				−0.261	0.272	0.321	−9.5	63.88	−5.93	0.532	0.15	0.215

a=0.181 m, h=0.08 m.

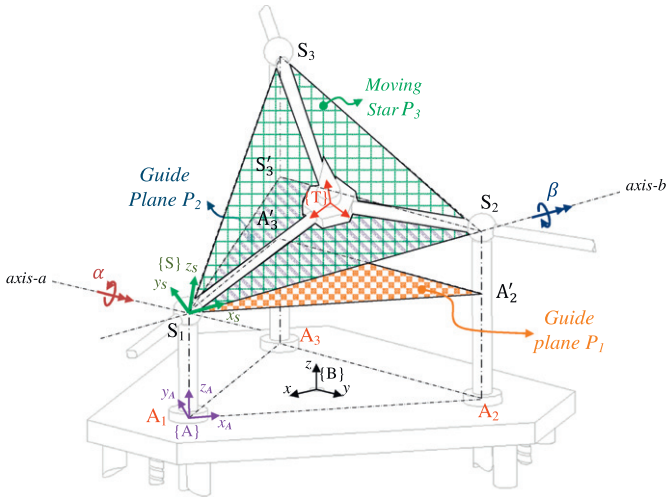

Fig. 10. Coordinate frames and guide planes to solve DirKin problem.

next be determined using the three points S_i. Fig. 10 shows guide planes and auxiliary coordinates frames required for solving the DirKin problem of the 3-PSP parallel robot.

Table 4
Transformation steps—{*S*} to {*B*}.

	Translation/rotation	Along/about	Coordinate frame	Value
Step #1	Translation	x	{*B*}	a
Step #2	Rotation	z	{*B*}	$5\pi/6$
Step #3	Translation	z_A	{*A*}	q_1
Step #4	Rotation	axis-a or y-axis	{*B*}	α
Step #5	Rotation	axis-b or x_S-axis	{*S*}	β

Consider two auxiliary coordinate frames {*A*} and {*S*} shown in Fig. 10. Origin of the fixed coordinate frame {*A*} is attached to the top fixed platform, at the point A_1. Its x- and z-axis are along the line connecting points A_1 to A_2 and z-axis of the fixed coordinate frame {*B*}, respectively. Origin of the moving coordinate frame {*S*} is attached to the point S_1 on the MS plane. Its x- and z-axis are along the line connecting points S_1 to S_2 and z-axis of the moving coordinate frame {*T*}, respectively. To transform frame {*S*} to frame {*B*}, two translations and three rotations are needed. To do this, two axes, axis-*a* and axis-*b* are defined which both pass through point S_1 but their directions are parallel to y-axis of {*B*} and x-axis of the frame {*S*}, respectively. Table 4 shows steps to transform frame {*S*} to frame {*B*}.

The transformation matrix, ${}^{B}_{S}\mathbf{T}$, which transfers frame $\{S\}$ to frame $\{B\}$ is define as

$$ {}^{B}_{S}\mathbf{T} = {}^{B}_{A}\mathbf{T}\,{}^{A}_{S}\mathbf{T} \tag{24} $$

where ${}^{A}_{S}\mathbf{T}$ and ${}^{A}_{S}\mathbf{T}$ are the transformation matrix which transfer frame $\{S\}$ to frame $\{A\}$ and frame $\{A\}$ to frame $\{B\}$, respectively. These matrices are defined as follow:

$$ {}^{B}_{A}\mathbf{T} = \begin{bmatrix} {}^{B}_{A}\mathbf{R} & {}^{B}_{A}\mathbf{t} \\ \mathbf{0}_{1\times 3} & 1 \end{bmatrix}, \quad {}^{A}_{S}\mathbf{T} = \begin{bmatrix} {}^{A}_{S}\mathbf{R} & {}^{A}_{S}\mathbf{t} \\ \mathbf{0}_{1\times 3} & 1 \end{bmatrix} \tag{25} $$

where ${}^{j}_{i}\mathbf{R}$ is a 3×3 rotation matrix which rotates frame $\{i\}$ to frame $\{j\}$, and ${}^{j}_{i}\mathbf{t}$ is a 3×1 vector that locates origin of $\{i\}$ relative to origin of $\{j\}$. These rotation matrices and vectors are expressed as

$$ {}^{B}_{A}\mathbf{R} = \mathbf{R}(z,\frac{5\pi}{6}) = \begin{bmatrix} \cos(5\pi/6) & -\sin(5\pi/6) & 0 \\ \sin(5\pi/6) & \cos(5\pi/6) & 0 \\ 0 & 0 & 1 \end{bmatrix}, \quad {}^{B}_{A}\mathbf{t} = \begin{bmatrix} a \\ 0 \\ 0 \end{bmatrix} \tag{26} $$

$$ {}^{A}_{S}\mathbf{R} = \mathbf{R}(y,\beta)\mathbf{R}(x,\alpha) = \begin{bmatrix} c\beta & s\beta s\alpha & s\beta c\alpha \\ 0 & c\alpha & -s\alpha \\ -s\beta & c\beta s\alpha & c\beta c\alpha \end{bmatrix}, \quad {}^{A}_{S}\mathbf{t} = \begin{bmatrix} 0 \\ 0 \\ q_1 \end{bmatrix} \tag{27} $$

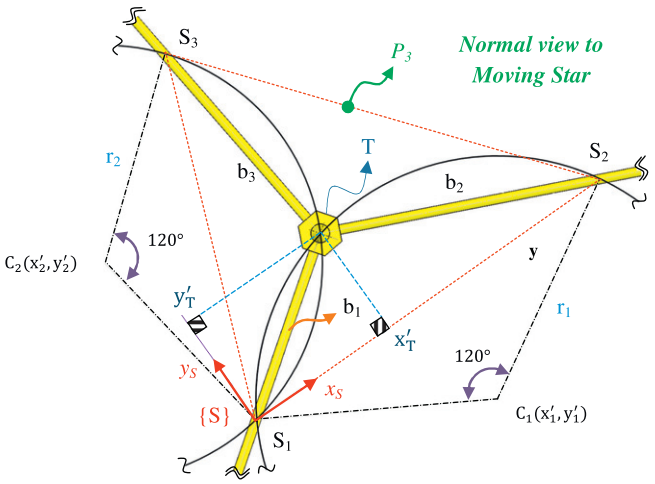

Fig. 11. Perpendicular view to the MS plane.

The tool position and orientation is more conveniently defined in $\{S\}$ which is why the direct kinematics solutions are first obtained in frame $\{S\}$. Using the transformation matrix, ${}^{B}_{S}\mathbf{T}$, vectors obtained in $\{S\}$ can be transferred to the fixed frame $\{B\}$. Then, the corresponding values of the Euler angles can be obtained using Eq. (6). Finally, by transferring the point T along the z-axis of frame $\{T\}$ by h, position of the tool tip, point P, which is the answer of DirKin problem is obtained. Fig. 11 shows the normal view, along z_S, of the MS plane. The center of the MS, point T, is situated on the MS plane. This plane, P_3, contains the three points, S_i. The location of point T in frame $\{S\}$, also located in x_S-y_S plane, can be obtained from intersection of two arcs S_1TS_3 and S_2TS_3. When a normal view of the MS, along z_S, is considered, the shape of the MS will always be in form of a symmetrical tripetalous star with 120° angles between any two branches. Therefore, upon obtaining position of points S_i and knowing that angles $\angle S_1C_1S_2$ and $\angle S_1C_2S_3$ are equal to 120°, center of two circles $C_1(x'_1,y'_1)$ and $C_2(x'_2,y'_2)$ with radiuses r_1 and r_2 can be obtained.

The equations of these two circles are defined as

$$ (x'-x'_1)^2+(y'-y'_1)^2 = r_1^2 \tag{28a} $$

$$ (x'-x'_2)^2+(y'-y'_2)^2 = r_2^2 \tag{28b} $$

Next, the position vector of point T, ${}^{S}\mathbf{t}$, can be obtained in the local frame $\{S\}$. This point is result of intersecting the two above circles. These two circles intersect each other at two points, S_1 and T. Therefore, there are two real answers for this set of equations. We know that base of auxiliary coordinate frame $\{S\}$ is always attached to point S_1. Therefore, one of the answers is zero (position of the point S_1 in local frame $\{S\}$, which is (0,0,0)). However, the second answer, the acceptable answer, is the position of point T in local frame $\{S\}$ as ${}^{S}\mathbf{t} = [x'_T \quad y'_T \quad 0]^T$. This answer can be transferred to fixed coordinate frame $\{B\}$ by using of the transformation matrix, Eq. (24). Therefore, position of the point T in frame $\{B\}$ can be obtained

$$ {}^{B}\mathbf{t} = {}^{B}_{S}\mathbf{T}\,{}^{S}\mathbf{t} \tag{29} $$

where ${}^{B}\mathbf{t} = [x_T \quad y_T \quad z_T]^T$ is position of the point T in frame $\{B\}$. Having the position of point T in frame $\{B\}$ and position of the three S-joints, S_i, we can obtain the length of each branch of MS, b_i, Eq. (18). Therefore, to obtain the position of the tool tip, point P, position of the point T is transferred along unit vector

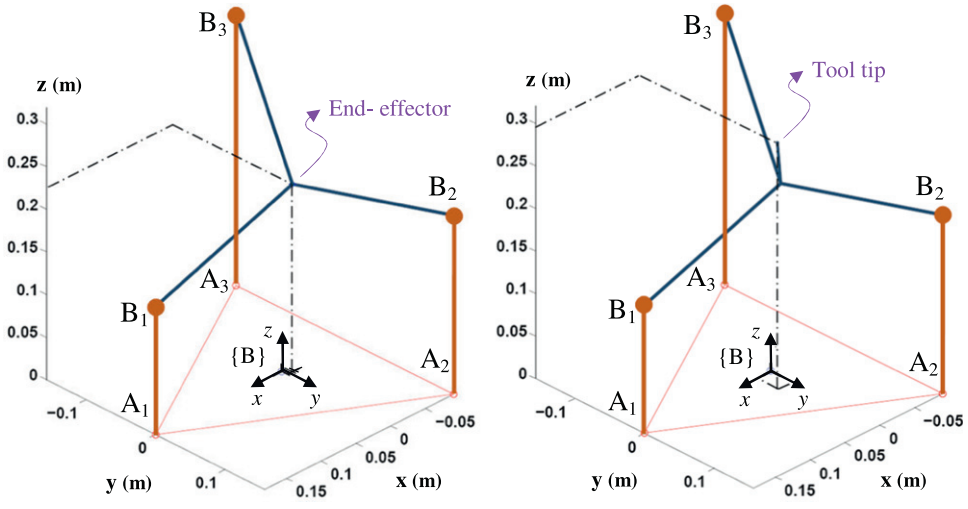

Fig. 12. Direct kinematics results.

Table 5
Inputs/outputs values of DirKin analysis.

	Inputs			Outputs								
	q_1 (m)	q_2 (m)	q_3 (m)	x_P (m)	y_P (m)	z_P (m)	θ (deg.)	ϕ (deg.)	λ (deg.)	b_1 (m)	b_2 (m)	b_3 (m)
Case #1	0.15	0.21	0.32	−0.003	0.012	0.224	−19.34	21.78	−3.75	0.198	0.169	0.213
Case #2	0.15	0.21	0.32	0.027	0.037	0.294	−19.34	21.78	−3.75	0.198	0.169	0.213

Case #1: a=0.181 m, h=0; Case #2: a=0.181 m, h=0.08 m.

$\widehat{\mathbf{s}}_{normal}$ which is previously defined in Eq. (13). Therefore, the position vector of the tool tip, (x_P,y_P,z_P), can be determined by rewriting Eq. (8) as

$$^{B}\mathbf{p} = {}^{B}\mathbf{t} + h\widehat{\mathbf{s}}_{normal} \tag{30}$$

Once b_i and (x_P,y_P,z_P) are calculated, the remaining output variables, the corresponding Euler angles (θ,φ,λ), can be calculated. To do this, similar to steps outlined for second mode of InvKin problem, Eqs. (22) and (23) are used. Next, similar to the InvKin section, two cases for the DirKin are considered. In the first case, the length of the tool is assumed to be zero while the second case assumes tool length of h=8 cm. Results are depicted in Fig. 12 and Table 5.

6. Jacobian analysis

In this section, Jacobian matrices describing relationship between the end-effector and the LRs velocity vectors are obtained. Using Jacobian matrices, singularity analysis and various kinds of singularities for the 3-PSP parallel robots are investigated. The acceleration inversion is also presented.

6.1. Velocity inversion

The kinematics constraint equations, Eq. (10), are defined in the base frame {B}. Therefore, for ith limb of the 3-PSP robot, both sides of the Eq. (10) can be time differentiated to yield

$$\dot{q}_i\widehat{\mathbf{q}}_i = \dot{b}_i\widehat{\mathbf{b}}_i + \boldsymbol{\omega_s}\times\mathbf{b}_i - \boldsymbol{\omega_s}\times\mathbf{h} + \mathbf{v}_P \quad \text{for } i=1,2,3 \tag{31}$$

where $\widehat{\mathbf{q}}_i$ and $\widehat{\mathbf{b}}_i$ are unit vectors along ith LRs and ith branch of the MS respectively. The values $\dot{q}_i$ and $\dot{b}_i$ represent the ith actuated joint rate and ith passive prismatic translational joint rate, respectively. Additionally, vectors ω_s and $\mathbf{v}_P$ denote angular velocity vector of the MS and Cartesian velocity vector of the tool tip, respectively. For brevity, in Eq. (10), the superscript "B" denoting the frame {B} in which vectors are defined in, is eliminated.

To eliminate the translational velocity vectors of the passive P joint, $\dot{b}_i\widehat{\mathbf{b}}_i$, both sides of Eq. (31) are dot multiplied with a specific vector which is perpendicular to the three vectors $\mathbf{b}_1$,$\mathbf{b}_2$ and $\mathbf{b}_3$. Additionally, as shown in Fig. 13, three unit vectors $\widehat{\mathbf{m}}_i$ which are all perpendicular to the MS plane can be defined as

$$\widehat{\mathbf{m}}_i = \frac{\mathbf{b}_i\times\mathbf{b}_j}{\|\mathbf{b}_i\times\mathbf{b}_j\|} \text{ for } i=1,2,3 \text{ and } j=2,3,1 \tag{32}$$

The three unit vectors $\widehat{\mathbf{m}}_i$ are perpendicular to the MS plane and therefore are also perpendicular to vectors $\mathbf{b}_i$. Then, by dot multiplying both sides of Eq. (31) with $\widehat{\mathbf{m}}_i$, the terms $\dot{b}_i\widehat{\mathbf{b}}_i$ can be eliminated. Then

$$\dot{q}_i\widehat{\mathbf{m}}_i\cdot\widehat{\mathbf{q}}_i = \dot{b}_i\widehat{\mathbf{m}}_i\cdot\widehat{\mathbf{b}}_i + \widehat{\mathbf{m}}_i\cdot(\boldsymbol{\omega_s}\times(\mathbf{b}_i-\mathbf{h})) + \widehat{\mathbf{m}}_i\cdot\mathbf{v}_P \quad \text{for } i=1,2,3 \tag{33}$$

where

$$\widehat{\mathbf{m}}_i \perp \widehat{\mathbf{b}}_i \quad \text{for } i=1,2,3 \tag{34}$$

Also, we know that

$$\mathbf{A}\cdot(\mathbf{B}\times\mathbf{C}) = (\mathbf{C}\times\mathbf{A})\cdot\mathbf{B} \tag{35}$$

Eq. (33) can be rewritten as follows:

$$\dot{q}_i\widehat{\mathbf{m}}_i\cdot\widehat{\mathbf{q}}_i = ((\mathbf{b}_i-\mathbf{h})\times\widehat{\mathbf{m}}_i)\cdot\boldsymbol{\omega_s} + \widehat{\mathbf{m}}_i\cdot\mathbf{v}_P \quad \text{for } i=1,2,3 \tag{36}$$

Finally, three scalar equations shown in Eq. (36) can be written in matrix form as follows:

$$\mathbf{J}_{inv}\dot{\mathbf{q}} = \mathbf{J}_{dir}\dot{\mathbf{X}} \tag{37}$$

where $\dot{\mathbf{q}} = [\dot{q}_1 \quad \dot{q}_2 \quad \dot{q}_3]^T$ and $\dot{\mathbf{X}} = [\mathbf{v}_P \quad \boldsymbol{\omega_s}]^T$ are vectors of the linear actuated joint rates and the MS velocities, respectively. Additionally, $\mathbf{v}_P = [\dot{x}_P \quad \dot{y}_P \quad \dot{z}_P]^T$ and $\boldsymbol{\omega_s} = [\dot{\theta} \quad \dot{\varphi} \quad \dot{\lambda}]^T$, represent translational and angular velocities of the MS, respectively. Therefore,

$$\mathbf{J}_{inv} = \begin{bmatrix} \widehat{\mathbf{m}}_1\cdot\widehat{\mathbf{q}}_1 & 0 & 0 \\ 0 & \widehat{\mathbf{m}}_2\cdot\widehat{\mathbf{q}}_2 & 0 \\ 0 & 0 & \mathbf{m}_3\cdot\widehat{\mathbf{q}}_3 \end{bmatrix}_{3\times3}, \quad \mathbf{J}_{dir} = \begin{bmatrix} \widehat{\mathbf{m}}_1{}^T & ((\mathbf{b}_1-\mathbf{h})\times\widehat{\mathbf{m}}_1)^T \\ \widehat{\mathbf{m}}_2{}^T & ((\mathbf{b}_2-\mathbf{h})\times\widehat{\mathbf{m}}_2)^T \\ \widehat{\mathbf{m}}_3{}^T & ((\mathbf{b}_3-\mathbf{h})\times\widehat{\mathbf{m}}_3)^T \end{bmatrix}_{3\times6} \tag{38}$$

where $\mathbf{J}_{inv}$ and $\mathbf{J}_{dir}$ are inverse and direct Jacobian matrices, respectively. In view of Eq. (37), we can rewrite

$$\dot{\mathbf{q}} = \mathbf{J}\dot{\mathbf{X}} \tag{39}$$

where $\mathbf{J} = \mathbf{J}_{inv}^{-1}\mathbf{J}_{dir}$ is a 3×6 matrix called overall Jacobian matrix of the 3-PSP parallel manipulator. Eq. (39) has many practical applications such as calculating the robot stiffness matrix [4,15] and robot dynamics. As stated before, the vector $\dot{\mathbf{X}}$, also known as twist vector, has three translational and three rotational speeds. Using Eq. (37) all 6 speed components of the MS are mapped to 3 speed components of LRs. However, the 3-PSP has only three DOFs and therefore only three of the six speed components in the twist vector, $\dot{\mathbf{X}}$, are independent and can be specified as inputs for the inverse velocity problem. Therefore, a new 3×3 Jacobian matrix is defined which maps the three desirable independent MS speed components to the three speed components of LRs. Then, one must first define which speeds are specified and eliminate the dependent speeds from Eq. (37).

Consider selecting $\dot{\theta}$, $\dot{\varphi}$ and $\dot{\lambda}$ as independent and $\dot{x}$,$\dot{y}$ and $\dot{z}$ as dependent MS speed variables, respectively. Then Eq. (37) can be re-written as

$$\mathbf{J}_{inv}\dot{\mathbf{q}} = \mathbf{J}_{dir\,X}\mathbf{v}_P + \mathbf{J}_{dir\,\Theta}\boldsymbol{\omega_s} \tag{40}$$

where $\boldsymbol{J}_{dir\,X}$ and $\boldsymbol{J}_{dir\,\Theta}$ are

$$\mathbf{J}_{dir\,X} = \begin{bmatrix} \widehat{\mathbf{m}}_1{}^T \\ \widehat{\mathbf{m}}_2{}^T \\ \widehat{\mathbf{m}}_3{}^T \end{bmatrix}_{3\times3}, \quad \mathbf{J}_{dir\,\Theta} = \begin{bmatrix} ((\mathbf{b}_1-\mathbf{h})\times\widehat{\mathbf{m}}_1)^T \\ ((\mathbf{b}_2-\mathbf{h})\times\widehat{\mathbf{m}}_2)^T \\ ((\mathbf{b}_3-\mathbf{h})\times\widehat{\mathbf{m}}_3)^T \end{bmatrix}_{3\times3} \tag{41}$$

To find the relationship between the angular velocities of the MS, ω_s, and the translational tool tip velocities, $\mathbf{v}_P$, both sides of Eq. (31) are dot multiplied with a specific unit vectors. These unit vectors, called as $\widehat{\mathbf{k}}_i$, are perpendicular to both $\dot{q}_i\widehat{\mathbf{q}}_i$ and $\dot{b}_i\widehat{\mathbf{b}}_i$ vectors and are shown in Fig. 14.

To define $\widehat{\mathbf{k}}_i$, three additional guide planes, called P_4, P_5 and P_6 are introduced. These three planes pass from three points A_i, T

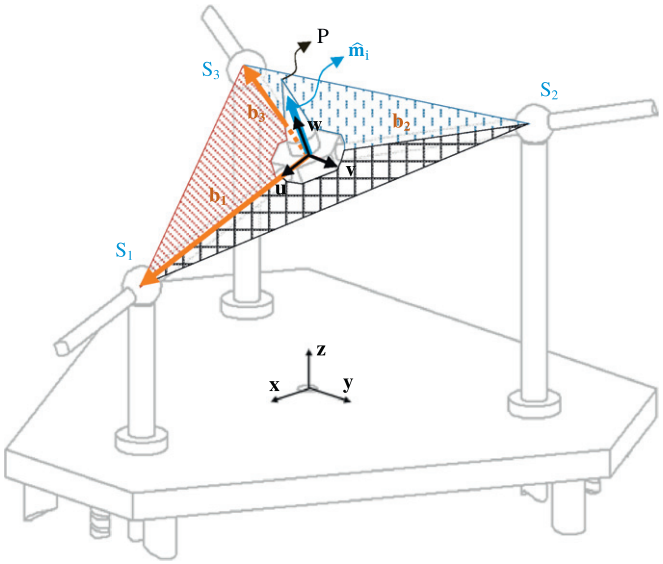

Fig. 13. Definition of the three unit vectors $\hat{\mathbf{m}}_i$.

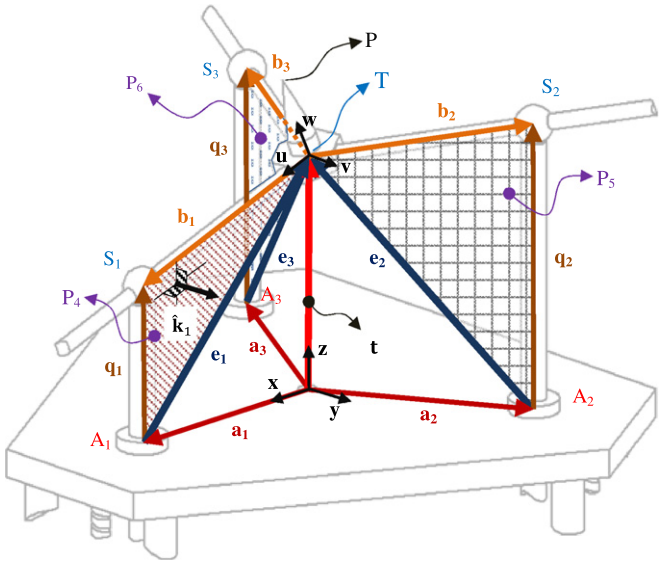

Fig. 14. Definition of the three unit vectors $\hat{\mathbf{k}}_i$.

and S_i, respectively. Therefore, we can write

$$\hat{\mathbf{k}}_i = \frac{\mathbf{e}_i \times \mathbf{q}_i}{\|\mathbf{e}_i \times \mathbf{q}_i\|} \quad \text{for } i = 1,2,3 \tag{42}$$

where vectors $\mathbf{e}_i$ connect points A_i to T and are expressed as

$$\mathbf{e}_i = \mathbf{T} - \mathbf{a}_i \qquad \text{for } i = 1,2,3 \tag{43}$$

Unit vectors $\hat{\mathbf{k}}_i$ are then perpendicular to planes containing the three vectors, $\mathbf{q}_i$, $\mathbf{e}_i$ and $\mathbf{b}_i$, respectively. Next to eliminate $\dot{\mathbf{q}}_i\hat{\mathbf{q}}_i$ and $\dot{b}_i\hat{\mathbf{b}}_i$ terms, both sides of Eq. (31) are dot multiplied with $\hat{\mathbf{k}}_i$, as

$$\dot{q}_i\hat{\mathbf{k}}_i\cdot\hat{\mathbf{q}}_i = \dot{b}_i\hat{\mathbf{k}}_i\cdot\hat{\mathbf{b}}_i + \hat{\mathbf{k}}_i\cdot(\boldsymbol{\omega}_s \times (\mathbf{b}_i - \mathbf{h})) + \hat{\mathbf{k}}_i\cdot\mathbf{v}_P \quad \text{for } i = 1,2,3 \tag{44}$$

where

$$\hat{\mathbf{k}}_i \perp \hat{\mathbf{b}}_i \text{ and } \hat{\mathbf{k}}_i \perp \hat{\mathbf{q}}_i \quad \text{for } i = 1,2,3 \tag{45}$$

Therefore, Eq. (44) is simplified as

$$\hat{\mathbf{k}}_i\cdot\mathbf{v}_P + ((\mathbf{b}_i - \mathbf{h}) \times \hat{\mathbf{k}}_i)\cdot\boldsymbol{\omega}_s = 0 \quad \text{for } i = 1,2,3 \tag{46}$$

Finally, three scalar equations shown in Eq. (46) are re-written in matrix form as

$$\mathbf{J}_{vp}\mathbf{v}_P + \mathbf{J}_{\omega s}\boldsymbol{\omega}_s = \mathbf{0} \tag{47a}$$

where

$$\mathbf{J}_{vp} = \begin{bmatrix} \hat{\mathbf{k}}_1^T \\ \hat{\mathbf{k}}_2^T \\ \hat{\mathbf{k}}_3^T \end{bmatrix}_{3\times3}, \quad \mathbf{J}_{\omega s} = \begin{bmatrix} ((\mathbf{b}_1 - \mathbf{h}) \times \hat{\mathbf{k}}_1)^T \\ ((\mathbf{b}_2 - \mathbf{h}) \times \hat{\mathbf{k}}_2)^T \\ ((\mathbf{b}_3 - \mathbf{h}) \times \hat{\mathbf{k}}_3)^T \end{bmatrix}_{3\times3} \tag{47b}$$

Therefore, Eq. (47a) can be re-written as

$$\mathbf{J}_c\dot{\mathbf{X}} = \mathbf{0}_{3\times1} \tag{48a}$$

where $\mathbf{J}_c = [\mathbf{J}_{vp} \quad \mathbf{J}_{\omega s}]$ is a 3×6 matrix called Jacobian of constraints for the 3-PSP parallel manipulator. The Jacobian of constraints matrix, $\mathbf{J}_c$, can be written as

$$\mathbf{J}_c = \begin{bmatrix} \hat{\mathbf{k}}_1^T & ((\mathbf{b}_1 - \mathbf{h}) \times \hat{\mathbf{k}}_1)^T \\ \hat{\mathbf{k}}_2^T & ((\mathbf{b}_2 - \mathbf{h}) \times \hat{\mathbf{k}}_2)^T \\ \hat{\mathbf{k}}_3^T & ((\mathbf{b}_3 - \mathbf{h}) \times \hat{\mathbf{k}}_3)^T \end{bmatrix}_{3\times6} \tag{48b}$$

Each row in the Jacobian of constraints matrix, represents a unit wrench of constraints imposed by the joints of a limb. This matrix will later, Section 7.4, be used to obtain related singularities when the moving platform has constrained motion.

6.1.1. *Non-pure rotational and translational Jacobian matrix*

In direct velocity inversion, $\dot{\mathbf{q}}_i$ are supplied and using Eq. (37), the three translational and rotational velocities of the MS are obtained. Conversely, in trajectory planning applications, the MS velocities are specified and motor speeds are obtained. The 3-PSP has three independent DOFs. Therefore, one must first decide which three of the six DOFs, operational modes, are used. For this purpose, non-pure rotational and non-pure translational modes of operation, $\theta\ \phi\ \lambda$ and XYZ, are considered and the relationships between independent velocities due to the MS in each mode and actuated joint rates are obtained. From Eqs. (40) and (47a), the relationship between the linear actuated joint rates, $\dot{\mathbf{q}}$, and the angular velocities of the MS, $\boldsymbol{\omega}_s$, can be calculated as

$$\mathbf{J}_{inv}\dot{\mathbf{q}} = \mathbf{J}_{rot}\boldsymbol{\omega}_s \tag{49}$$

where $\mathbf{J}_{rot} = (\mathbf{J}_{dir\ X}\mathbf{J}_{vp}^{-1}\mathbf{J}_{\omega s} + \mathbf{J}_{dir\ \Theta})$ is a 3×3 matrix and is called non-pure rotational Jacobian matrix. Additionally, the relationship between the linear actuated joint rates, $\dot{\mathbf{q}}$, and the translational tool tip velocity, $\mathbf{v}_P$, can be expressed as

$$\mathbf{J}_{inv}\dot{\mathbf{q}} = \mathbf{J}_{trans}\mathbf{v}_P \tag{50}$$

where $\mathbf{J}_{trans} = (\mathbf{J}_{dir\ X} + \mathbf{J}_{dir\ \Theta}\mathbf{J}_{\omega s}^{-1}\mathbf{J}_{vp})$ is also a 3×3 matrix and is called non-pure translational Jacobian matrix. There are several advantages in splitting the overall Jacobian of constraint matrix and obtaining Eqs. (49) and (50). The resulting square, 3×3, non-pure rotational and non-pure translational Jacobian matrices will now better enable trajectory planning as well as obtaining the singularities in non-pure rotational and non-pure translational modes, respectively.

6.2. *Acceleration inversion*

In this subsection, the relationship between the translational and angular acceleration of the MS and the LRs velocity vectors are obtained. To do this, both sides of Eq. (31) are time differentiated to yield:

$$\begin{aligned}\ddot{q}_i\hat{\mathbf{q}}_i = {} & (\ddot{\mathbf{b}}_i\hat{\mathbf{b}}_i + \boldsymbol{\omega}_s \times \dot{\mathbf{b}}_i\hat{\mathbf{b}}_i) + (\dot{\boldsymbol{\omega}}_s \times \mathbf{b}_i + \boldsymbol{\omega}_s \times \dot{b}_i\hat{\mathbf{b}}_i + \boldsymbol{\omega}_s(\boldsymbol{\omega}_s \times \mathbf{b}_i)) \\ & -(\dot{\boldsymbol{\omega}}_s \times \mathbf{h} + \boldsymbol{\omega}_s \times (\boldsymbol{\omega}_s \times \mathbf{h})) + \dot{\mathbf{v}}_P \quad \text{for } i = 1,2,3\end{aligned} \tag{51}$$

The values $\ddot{\mathbf{q}}_i$ and $\ddot{\mathbf{b}}_i$ represent the ith actuated joint acceleration and ith passive prismatic joint linear acceleration, respectively.

Additionally, vectors $\dot{\boldsymbol{\omega}}_{\boldsymbol{s}}$ and $\dot{\mathbf{v}}_P$ denote angular acceleration vector of the MS and Cartesian acceleration vector for the tool tip, respectively. We know that

$$\mathbf{A}\times(\mathbf{B}\times\mathbf{C})=(\mathbf{A}.\mathbf{C})\mathbf{B}-(\mathbf{A}.\mathbf{B})\mathbf{C} \text{ and } \mathbf{A}\times\mathbf{B}=-\mathbf{B}\times\mathbf{A} \tag{52}$$

Using above relations, Eq. (51) can be rewritten as follows:

$$\ddot{q}_i\hat{\mathbf{q}}_i=\ddot{b}_i\hat{\mathbf{b}}_i+2\boldsymbol{\omega}_{\boldsymbol{s}}\times\dot{b}_i\hat{\mathbf{b}}_i+\dot{\boldsymbol{\omega}}_{\boldsymbol{s}}\times(\mathbf{b}_i-\mathbf{h})+(\boldsymbol{\omega}_{\boldsymbol{s}}.(\mathbf{b}_i-\mathbf{h}))\boldsymbol{\omega}_{\boldsymbol{s}} -(\boldsymbol{\omega}_{\boldsymbol{s}}.\boldsymbol{\omega}_{\boldsymbol{s}})(\mathbf{b}_i-\mathbf{h})+\dot{\mathbf{v}}_P \quad \text{for } i=1,2,3 \tag{53}$$

By substituting vector $\dot{b}_i\hat{\mathbf{b}}_i$ from Eq. (31) into above equation, we will have

$$\ddot{q}_i\hat{\mathbf{q}}_i=\ddot{b}_i\hat{\mathbf{b}}_i+2\boldsymbol{\omega}_{\boldsymbol{s}}\times\dot{q}_i\hat{\mathbf{q}}_i-2\boldsymbol{\omega}_{\boldsymbol{s}}\times(\boldsymbol{\omega}_{\boldsymbol{s}}\times(\mathbf{b}_i-\mathbf{h}))-2\boldsymbol{\omega}_{\boldsymbol{s}}\times\mathbf{v}_P+\dot{\boldsymbol{\omega}}_{\boldsymbol{s}}\times(\mathbf{b}_i-\mathbf{h}) +(\boldsymbol{\omega}_{\boldsymbol{s}}.(\mathbf{b}_i-\mathbf{h}))\boldsymbol{\omega}_{\boldsymbol{s}}-(\boldsymbol{\omega}_{\boldsymbol{s}}.\boldsymbol{\omega}_{\boldsymbol{s}})(\mathbf{b}_i-\mathbf{h})+\dot{\mathbf{v}}_P \quad \text{for } i=1,2,3 \tag{54}$$

Consider relationship (52), we can rewrite the above equation as

$$\ddot{q}_i\hat{\mathbf{q}}_i=\ddot{b}_i\hat{\mathbf{b}}_i+2\boldsymbol{\omega}_{\boldsymbol{s}}\times\dot{q}_i\hat{\mathbf{q}}_i-2\boldsymbol{\omega}_{\boldsymbol{s}}\times\mathbf{v}_P+\dot{\boldsymbol{\omega}}_{\boldsymbol{s}}\times(\mathbf{b}_i-\mathbf{h})-((\boldsymbol{\omega}_{\boldsymbol{s}}.(\mathbf{b}_i-\mathbf{h}))\boldsymbol{\omega}_{\boldsymbol{s}} +(\boldsymbol{\omega}_{\boldsymbol{s}}.\boldsymbol{\omega}_{\boldsymbol{s}})(\mathbf{b}_i-\mathbf{h})+\dot{\mathbf{v}}_P \quad \text{for } i=1,2,3 \tag{55}$$

To eliminate the linear acceleration vectors of the passive prismatic joint, $\ddot{b}_i\hat{\mathbf{b}}_i$, both sides of Eq. (55) are dot multiplied with unit vectors, $\hat{\mathbf{m}}_i$, defined in Eq. (32). We can write

$$\ddot{q}_i\hat{\mathbf{m}}_i.\hat{\mathbf{q}}_i=((\mathbf{b}_i-\mathbf{h})\times\hat{\mathbf{m}}_i).\dot{\boldsymbol{\omega}}_{\boldsymbol{s}}+\hat{\mathbf{m}}_i.\dot{\mathbf{v}}_P+2((\dot{q}_i\hat{\mathbf{q}}_i\times\hat{\mathbf{m}}_i)-(\mathbf{v}_P\times\hat{\mathbf{m}}_i)).\boldsymbol{\omega}_{\boldsymbol{s}} +(\boldsymbol{\omega}_{\boldsymbol{s}}.\boldsymbol{\omega}_{\boldsymbol{s}})\hat{\mathbf{m}}_i.(\mathbf{b}_i-\mathbf{h})-(\boldsymbol{\omega}_{\boldsymbol{s}}.(\mathbf{b}_i-\mathbf{h}))\hat{\mathbf{m}}_i.\boldsymbol{\omega}_{\boldsymbol{s}} \quad \text{for } i=1,2,3 \tag{56}$$

Finally, the three above scalar equations can be written in matrix form as follows:

$$\mathbf{J}_{inv}\ddot{\mathbf{q}}=\mathbf{J}_{dir}\ddot{\mathbf{X}}+\mathbf{N}\boldsymbol{\omega}_{\boldsymbol{s}}+\mathbf{M} \tag{57}$$

where $\ddot{\mathbf{q}}=[\ddot{q}_1 \quad \ddot{q}_2 \quad \ddot{q}_3]^T$ and $\ddot{\mathbf{X}}=[\dot{\mathbf{v}}_P \quad \boldsymbol{\omega}_{\boldsymbol{s}}]^T$ are the actuated joints and MS acceleration vectors, respectively. Additionally, $\dot{\mathbf{v}}_P=[\ddot{x} \quad \ddot{y} \quad \ddot{z}]^T$ and $\dot{\boldsymbol{\omega}}_{\boldsymbol{s}}=[\ddot{\theta} \quad \ddot{\varphi} \quad \ddot{\lambda}]^T$ represent linear and angular accelerations of the MS, respectively. Finally, the matrices $\mathbf{N}$ and $\mathbf{M}$ are defined as

$$\mathbf{N}=\begin{bmatrix}2((\dot{q}_1\hat{\mathbf{q}}_1\times\hat{\mathbf{m}}_1)-(\mathbf{v}_P\times\hat{\mathbf{m}}_1))^T\\2((\dot{q}_2\hat{\mathbf{q}}_2\times\hat{\mathbf{m}}_2)-(\mathbf{v}_P\times\hat{\mathbf{m}}_2))^T\\2((\dot{q}_3\hat{\mathbf{q}}_3\times\hat{\mathbf{m}}_3)-(\mathbf{v}_P\times\hat{\mathbf{m}}_3))^T\end{bmatrix}_{3\times3},$$
$$\mathbf{M}=\begin{bmatrix}(\boldsymbol{\omega}_{\boldsymbol{s}}.\boldsymbol{\omega}_{\boldsymbol{s}})\hat{\mathbf{m}}_1.(\mathbf{b}_1-\mathbf{h})-(\boldsymbol{\omega}_{\boldsymbol{s}}.(\mathbf{b}_1-\mathbf{h}))\hat{\mathbf{m}}_1.\boldsymbol{\omega}_{\boldsymbol{s}}\\(\boldsymbol{\omega}_{\boldsymbol{s}}.\boldsymbol{\omega}_{\boldsymbol{s}})\hat{\mathbf{m}}_2.(\mathbf{b}_2-\mathbf{h})-(\boldsymbol{\omega}_{\boldsymbol{s}}.(\mathbf{b}_2-\mathbf{h}))\hat{\mathbf{m}}_2.\boldsymbol{\omega}_{\boldsymbol{s}}\\(\boldsymbol{\omega}_{\boldsymbol{s}}.\boldsymbol{\omega}_{\boldsymbol{s}})\hat{\mathbf{m}}_3.(\mathbf{b}_3-\mathbf{h})-(\boldsymbol{\omega}_{\boldsymbol{s}}.(\mathbf{b}_3-\mathbf{h}))\hat{\mathbf{m}}_3.\boldsymbol{\omega}_{\boldsymbol{s}}\end{bmatrix}_{3\times1} \tag{58}$$

Upon completion of velocity inversion analysis, all speed components of both MS and actuators are determined. Therefore, Eq. (57) provides the relationship between angular and linear acceleration of the MS with linear acceleration of the three actuators.

7. Singularity analysis

In singular configuration, the mobile platform may instantaneously gain one or more unconstrained degrees of freedom. Therefore, in singular configurations, one or more DOFs of the moving platform are not controllable. Singularities are undesirable situations in manipulator operation for both motion and force control. For example, in some singular configurations; the moving platform can have motion even if all actuated joints are locked. Trajectory planning is another application where singularity information is used. Clearly, trajectories that do not pass or come close to singular points are desirable.

Singularity limits and separates the workspace of a mechanism. Therefore, a usable robot workspace may be obtained by eliminating all the singular configurations from the theoretical workspace. The simplified velocity relation introduced in Eq. (39) can be used in deriving the singularity equation of the parallel manipulators. Algebraically, a singularity occurs when the overall Jacobian matrix, $\mathbf{J}$, Eq. (39), is not of full rank or when the determinant of this matrix becomes zero. However, using the overall Jacobian matrix to analytically determine the singularity equations is difficult. To overcome this, the traditional form of velocity relation, Eq. (37), is used which allows finding the singularity conditions.

In this paper, the singularities of the 3-PSP are classified into three categories which are defined by when $\mathbf{J}_{inv}$, $\mathbf{J}_{dir}$ or both become singular. Additionally, the constraint singularity using Eqs. (48a) and (48b) is derived and singular configurations is investigated.

7.1. The first type of singularity—Inverse Kinematic Singularity (IKS)

This type of singularity, called IKS, occurs whenever $\mathbf{J}_{inv}$ becomes singular but $\mathbf{J}_{dir}$ is invertible. As shown in Eq. (38), matrix $\mathbf{J}_{inv}$ is a square matrix while matrix $\mathbf{J}_{dir}$ is not. The first type of singularity occurs when

$$\det(\mathbf{J}_{inv})=0 \text{ , but } \mathrm{Rank}(\mathbf{J}_{dir})=3 \text{ (full rank)}$$

From Eq. (38) this condition requires

$$\hat{\mathbf{m}}_i\cdot\hat{\mathbf{q}}_i=0 \quad \text{for } i=1 \text{ or } 2 \text{ or } 3$$

There are three conditions that can fulfill the above relation. These include, when either $\hat{\mathbf{m}}_i$, or $\hat{\mathbf{q}}_i$ are zero or both $\hat{\mathbf{m}}_i$ and $\hat{\mathbf{q}}_i$ are perpendicular to each other. The values of the unit vectors $\hat{\mathbf{m}}_i$ and $\hat{\mathbf{q}}_i$ by definition are not zero. The only remaining condition is when both unit vectors $\hat{\mathbf{m}}_i$ and $\hat{\mathbf{q}}_i$ are perpendicular to each other. Theoretically, this condition can occur whenever one of the LR's lengths becomes infinite. In reality, because the motions of the LRs are limited, this condition cannot occur. Therefore the first type of singularity does not occur for the 3-PSP robot.

7.2. The second type of singularity—Direct Kinematic Singularity (DKS)

This type of singularity, called DKS, occurs whenever $\mathbf{J}_{dir}$ becomes singular but $\mathbf{J}_{inv}$ is invertible. The second type of singularity occurs when

$$\det(\mathbf{J}_{inv})\neq0, \text{ but } \mathrm{Rank}(\mathbf{J}_{dir})<3$$

Note that $\mathbf{J}_{dir}$ is not a square matrix and if $\mathrm{Rank}(\mathbf{J}_{dir})=3$ then $\mathbf{J}_{dir}$ is a full rank. Therefore, the second type of singularity occurs whenever rank of matrix $\mathbf{J}_{dir}$ is equal to 1 or 2. Theoretically, this type of configuration is reached whenever two rows of $\mathbf{J}_{dir}$ are linearly dependent. First, consider unit vector $\hat{\mathbf{m}}_i$ in matrix $\mathbf{J}_{dir}$. By inspection of Eq. (32), we can see that the unit vectors $\hat{\mathbf{m}}_i$ in matrix $\mathbf{J}_{dir}$ are parallel. Therefore, these unit vectors are always linearly dependent.

Next, consider vectors $(\mathbf{b}_i-\mathbf{h})\times\hat{\mathbf{m}}_i$ in matrix $\mathbf{J}_{dir}$. If two of three vectors $(\mathbf{b}_i-\mathbf{h})\times\hat{\mathbf{m}}_i$ are also parallel then two rows of the matrix $\mathbf{J}_{dir}$ will be linearly dependent. Therefore, if the second condition was to hold, then matrix $\mathbf{J}_{dir}$ will not be full rank. However, the structure of the MS does not allow any two of three vectors $(\mathbf{b}_i-\mathbf{h})\times\hat{\mathbf{m}}_i$ to be parallel. Therefore the second type of singularity also does not occur for the 3-PSP robot.

7.3. The third type of singularity—Combined Singularity (CS)

This type of singularity, called CS, occurs whenever both $\mathbf{J}_{inv}$ and $\mathbf{J}_{dir}$ simultaneously become singular. For this purpose, the third type of singularity occurs when:

$$\det(\mathbf{J}_{inv})=0 \text{ and } \mathrm{Rank}(\mathbf{J}_{dir})<3$$

Generally, this type of singularity can occur only for manipulator with special kinematic architecture and it has a slightly different nature than the first two since it depends on the configuration and the architecture of the manipulator [1]. We have this type of singularity whenever the two previously

defined singularities occur simultaneously. Therefore, from Eq. (38) this requirement implies,

$$\det(\mathbf{J}_{inv}) = 0 \Rightarrow \hat{\mathbf{m}}_i \cdot \hat{\mathbf{q}}_i = 0 \quad \text{for } i = 1 \text{ or } 2 \text{ or } 3$$

$$\text{Rank}(\mathbf{J}_{dir}) < 3 \Rightarrow \begin{cases} \hat{\mathbf{m}}_i = 0, \text{ for } i = 1 \text{ or } 2 \text{ or } 3 \\ \text{or,} \\ (i\text{th row of } \mathbf{J}_{dir}) = (j\text{th row of } \mathbf{J}_{dir}) \end{cases}$$

If the two above requirements occur simultaneously, the third type of singularity will occur. For this purpose, one of the three vectors $\hat{\mathbf{m}}_i$ must have zero components. However, this condition also does not occur as $\hat{\mathbf{m}}_i$ is a unit vector and cannot be zero.

7.4. Constraint singularity

The constraint singularity occurs whenever $\mathbf{J}_c$ become singular [31,32]. For this purpose, this type of singularity occurs when:

$$\text{Rank}(\mathbf{J}_c) < 3$$

As shown in Eq. (48b), this type of singularity can occur whenever any one of the two following conditions is met:

Condition #1: One of three unit vectors $\hat{\mathbf{k}}_i$ has zero components. This cannot occur as $\hat{\mathbf{k}}_i$ are unit vectors and cannot be zero.
Condition #2: Two rows of matrix $\mathbf{J}_c$ are linearly dependent. This can occur whenever two of three unit vectors $\hat{\mathbf{k}}_i$ are linearly dependent and the corresponding two of the three vectors $(\mathbf{b}_i - \mathbf{h}) \times \hat{\mathbf{k}}_i$ are also linearly dependent. This can occur when tool length is zero, $h=0$, and all three guide planes P_4, P_5 and P_6 are perpendicular to the top fixed platform $\Delta A_1A_2A_3$. This implies the lengths of all three LRs are equal, $(\mathbf{q}_1 = \mathbf{q}_2 = \mathbf{q}_3)$ (see Fig. 15(a)). To better explain this singularity concept of force is used. As shown in Fig. 15(b), forces in x-direction are not experienced by the motors of the 2-link robot. Similarly, as shown in Fig. 15(c), forces in x- and y-directions are not experienced by motors of the 3-PSP.

Additionally, we can conclude that when the constraint singularity occur, both $\mathbf{J}_{rot} = (\mathbf{J}_{dir\,X}\mathbf{J}_{vp}^{-1}\mathbf{J}_{\omega s} + \mathbf{J}_{dir\,\Theta})$ and $\mathbf{J}_{trans} = (\mathbf{J}_{dir\,X} + \mathbf{J}_{dir\,\Theta}\mathbf{J}_{\omega s}^{-1}\mathbf{J}_{vp})$ are not computable. These conditions occur whenever $\det(\mathbf{J}_{vp}) = 0$ and $\det(\mathbf{J}_{\omega s}) = 0$.

8. Workspace analysis of 3-PSP parallel robot

The workspace of the 3-PSP can be determined based on the required application. For example, one may choose the non-pure translation, non-pure orientation, or the coupled mixed-type workspace. In this section two modes of operation are selected, *XYZ* and $\theta\varphi Z$, and the reachable workspaces is obtained using a numerical approach based on discretization of the MS variables. The robot parameters of a_i and h are considered to be 181 mm and 80 mm, respectively. Additionally, the range of LRs motion is considered to be $0 \le q_i \le 40$ cm. The InvKin solution for each Cartesian node is calculated and robot workspace is obtained. The following algorithm is used:

Algorithm#1 for obtaining the workspace using InvKin
For $z_P = 0$ to 40 cm, step size = 2 cm (20 layers)
  For $x_P = -10$ to 10 cm, step size = 0.1 cm
    or $\theta = 75^\circ$ to -75°, step size = 1°
    For $y_P = -10$ to 10 cm, step size = 0.1 cm
      or $\varphi = 75^\circ$ to -75°, step size = 1°

Solve Invkin of the 3-PSP parallel manipulator
(Calculate q_i, b_i, λ and θ, φ or x_P, y_P using inverse kinematics)
If $0 \le q_i \le 40$ cm and error $\le 10^{-5}$ cm
  x_P, y_P or θ, φ are on the workspace
Else, are not on the workspace;
End if

  End
End
End

Note that, the range considered for values x_P and y_P as well as θ and ϕ used by the algorithm are larger than, the limit allowed by

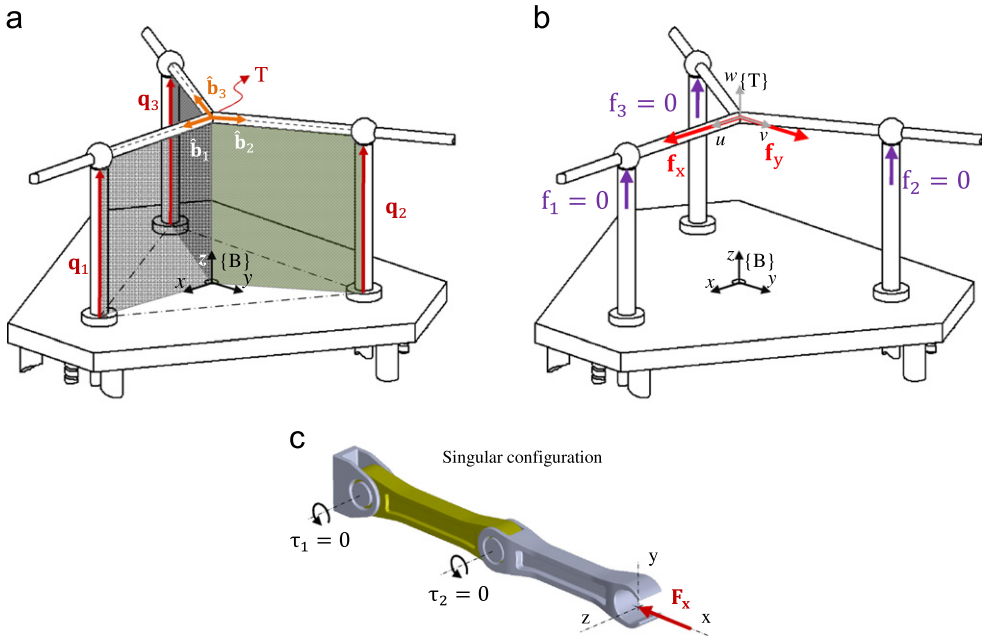

Fig. 15. The inverse non-pure translational singularity: (a) singular configuration, condition #2, (b) concept of non-pure translational singularity using force as explanation, and (c) 2-link robot in singular configuration.

the robot. The larger range insures all points are included in available workspace for the robot.

A second method for obtaining workspace based on DirKin is also presented. In Section 5, we showed that DirKin of this chain has a unique solution. This important property of the 3-PSP is used to obtain the workspaces. For this purpose another numerical algorithm, is presented

Algorithm#2 for obtaining the workspace using DirKin
For $q_1=0$ to 40 cm, step size=0.1 cm
  For $q_2=0$ to 40 cm, step size=0.1 cm
    For $q_3=0$ to 40 cm, step size=0.1 cm
Direct kinematics of the 3-PSP parallel manipulator
(Calculate x_P,y_P,z_P and θ, φ using direct kinematics)
    End
  End
End

Using the second algorithm, there is no need to filter the answers because all answers are within the workspace. The reachable workspace related to rotational and translational parameters of MS, (θ,ϕ,z_P), is shown in Fig. 16(a). Additionally, the reachable workspace related to translational parameters of tool tip, (x_P,y_P,z_P), both with and without considering length of the tool, h, is shown in Figs. 16(b) and (c).

Consider Figs. 16(a) and (b). A direct comparison between the two workspaces cannot be made due to the different units used for the axis. However, comparison between these two graphs provides a perspective for the range of motion in its corresponding workspace. Using this viewpoint, we may conclude that the ranges of values (motion) for variables in the $\theta\phi Z$ workspace are significantly larger than the corresponding XYZ workspace. Furthermore, as expected, there is no control on MS orientation in the XYZ mode, therefore it is possible that small changes in XYZ variables result in large changes in MS orientation. Therefore, we can conclude that the 3-PSP is better

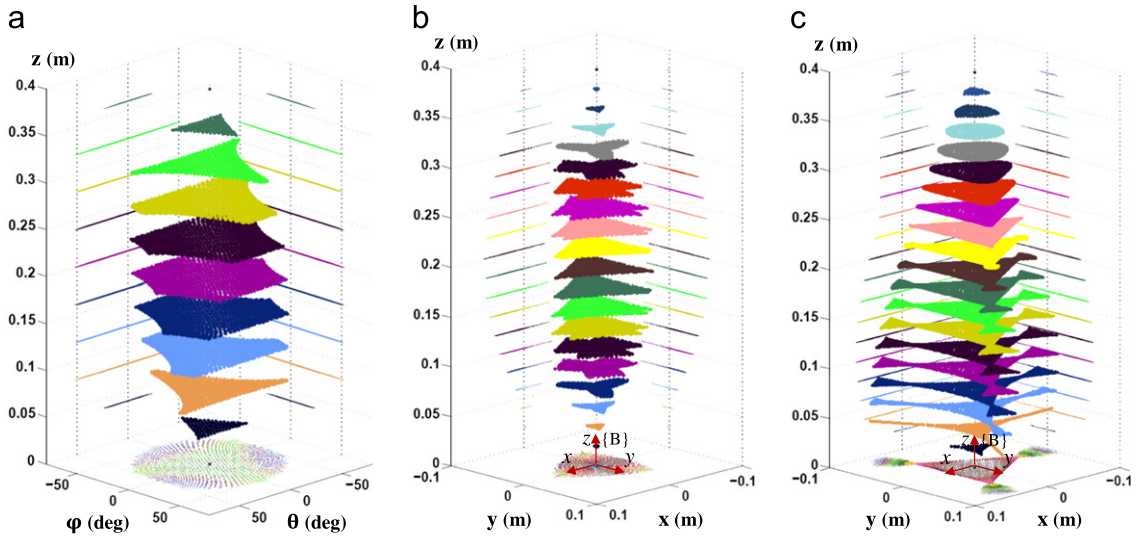

Fig. 16. Reachable workspace: (a) coupled mixed-type workspace (R2T1, θ,ϕ,z_P), (b) non-pure translation workspace (x_P,y_P,z_P) without tool, $h=0$ and (c) non-pure translation workspace (x_P,y_P,z_P) with tool, $h=0.08$ m.

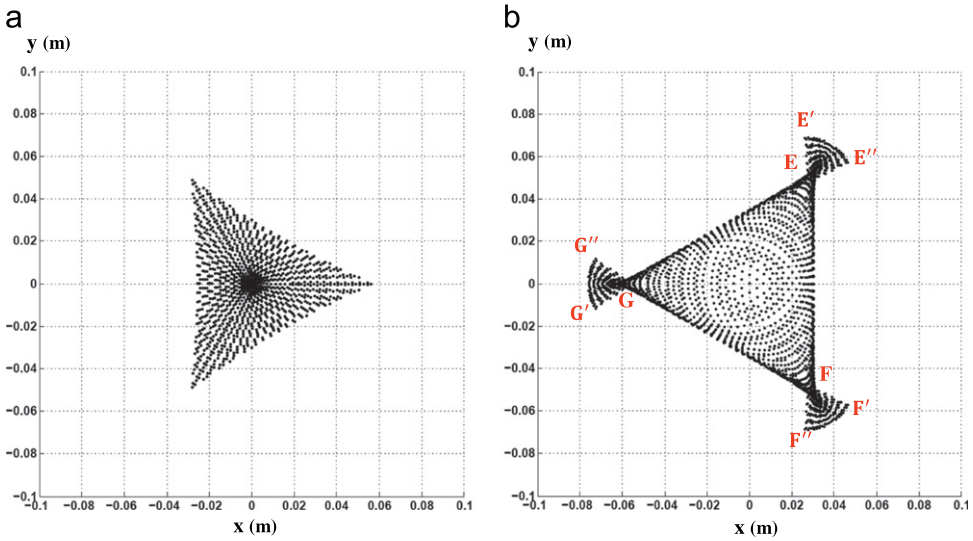

Fig. 17. Reachable workspace related to translational parameters of tool tip (x_P,y_P,z_P) in plane $z_P=20$ cm: (a) without tool, $h=0$ and (b) with tool, $h=8$ cm.

suited to be operated in the $\theta\ \phi\ Z$ mode. The effect of adding a tool with specific height, $h=8$ cm, on the *XYZ* workspace is also investigated (see Figs. 16(b) and (c)). At the first glance, one may conclude that the workspace is significantly enlarged. However, consider the reachable workspace obtained in plane $z_P=20$ cm (see Fig. 17(a) and (b)). As can be seen, even though the overall workspace area is increased, from Figs. 17(a) and (b), the effective area is only slightly increased. In Fig. 17(b), the robot is restricted to pass through point E, F and G in order to reach its full potential. Therefore, the internal triangle ΔEFG is its effective workspace which is only slightly larger than triangle in Fig. 17(a).

9. Conclusion

A spatial type of the 3-PSP parallel manipulator with specific architecture is introduced. The robot has three degrees of freedom which can be selected among the six, x,y,z,θ,φ and λ, MS variables. Two modes of operations, $\theta\phi Z$ and *XYZ*, are considered. For these two modes, position and workspace analysis is thoroughly presented. For the direct kinematics, a geometrical approach yielding a unique solution is presented. For the inverse kinematics, a closed form solution for the *XYZ* mode yielding to two answers is presented. Two examples for InvKin and one example for DirKin problem are supplied. In each example, two states of with and without tool height are studied and graphically illustrated. Next, velocity and acceleration inversions are presented in invariant form and the non-pure rotational and non-pure translational Jacobian matrices are defined to derive the relationship between angular and translational velocities of the moving platform and the actuated joint rates. Additionally, using non-pure rotational and non-pure translational Jacobian matrices, Jacobian of constraint is defined. The three types of conventional singularities are analyzed. The analysis shows that, the 3-PSP robot is free of the three conventional, architecture singularities. Additionally, the constraint singularity analysis is presented for the 3-PSP robot using Jacobian of constraint. It is shown that the 3-PSP parallel robot has a constraint singularity when the lengths of all three LRs are equal.

Finally, the robot reachable workspaces are determined. It is shown that the ranges of motion for variables in the $\theta\varphi Z$ workspace are significantly larger than the corresponding *XYZ* workspace. Furthermore, the $\theta\varphi Z$ mode is free of singularities. It is therefore, concluded that the 3-PSP is better suited to be operated in the $\theta\varphi Z$ mode.

The main contributions of this paper are, obtaining an analytical solution for the Invkin in *XYZ* mode, obtaining a numerical solution for the Invkin in $\theta\varphi Z$ mode, obtaining an analytical solution for Dirkin with unique solution, presenting the velocity and acceleration inversion, obtaining the direct and inverse Jacobians, Jacobian of constraints as well as introducing non-pure rotational and non-pure translational Jacobian matrices, investigating the conventional types of singularities as well as constraint singularity using the Jacobian of constraints matrix, presenting two methods for obtaining robot workspaces in two operational modes and finally investigating the effect of tool length on the *XYZ* workspace.

Appendix A

Extracting Eq. (10) and substituting rotation matrix components from Eq. (6), we can obtain a set of 9 nonlinear algebraic equations called constraint equations as

$$\psi(q)=0 \tag{A.1}$$

where

$$\begin{aligned}
\psi_1 &= x_P + b_1(\cos(\varphi)\cos(\lambda)) - h(\sin(\theta)\sin(\lambda)+\sin(\varphi)\cos(\theta)\cos(\lambda)) - a = 0\\
\psi_2 &= y_P + b_1(\cos(\varphi)\sin(\lambda)) - h(-\sin(\theta)\cos(\lambda)+\sin(\varphi)\cos(\theta)\sin(\lambda)) = 0\\
\psi_3 &= z_P + b_1(-\sin(\varphi)) - h(\cos(\varphi)\cos(\theta)) - q_1 = 0\\
\psi_4 &= x_P - \frac{1}{2}b_2(\cos(\varphi)\cos(\lambda)) + \frac{\sqrt{3}}{2}b_2(-\cos(\theta)\sin(\lambda)+\sin(\varphi)\sin(\theta)\cos(\lambda))\\
&\quad - h(\sin(\theta)\sin(\lambda)+\sin(\varphi)\cos(\theta)\cos(\lambda)) + \frac{1}{2}a = 0\\
\psi_5 &= y_P - \frac{1}{2}b_2(\cos(\varphi)\sin(\lambda)) + \frac{\sqrt{3}}{2}b_2(\cos(\theta)\cos(\lambda)+\sin(\varphi)\sin(\theta)\sin(\lambda))\\
&\quad - h(-\sin(\theta)\cos(\lambda)+\sin(\varphi)\cos(\theta)\sin(\lambda)) - \frac{\sqrt{3}}{2}a = 0\\
\psi_6 &= z_P - \frac{1}{2}b_2(-\sin(\varphi)) + \frac{\sqrt{3}}{2}b_2(\cos(\varphi)\sin(\theta)) - h(\cos(\varphi)\cos(\theta)) - q_2 = 0\\
\psi_7 &= x_P - \frac{1}{2}b_3(\cos(\varphi)\cos(\lambda)) - \frac{\sqrt{3}}{2}b_3(-\cos(\theta)\sin(\lambda)+\sin(\varphi)\sin(\theta)\cos(\lambda))\\
&\quad - h(\sin(\theta)\sin(\lambda)+\sin(\varphi)\cos(\theta)\cos(\lambda)) + \frac{1}{2}a = 0\\
\psi_8 &= y_P - \frac{1}{2}b_3(\cos(\varphi)\sin(\lambda)) - \frac{\sqrt{3}}{2}b_3(\cos(\theta)\cos(\lambda)+\sin(\varphi)\sin(\theta)\sin(\lambda))\\
&\quad - h(-\sin(\theta)\cos(\lambda)+\sin(\varphi)\cos(\theta)\sin(\lambda)) + \frac{\sqrt{3}}{2}a = 0\\
\psi_9 &= z_P - \frac{1}{2}b_3(-\sin(\varphi)) - \frac{\sqrt{3}}{2}b_3(\cos(\varphi)\sin(\theta)) - h(\cos(\varphi)\cos(\theta)) - q_3 = 0
\end{aligned} \tag{A.2}$$

References

[1] Li Y, Xu Q. Kinematic analysis of a 3-PRS parallel manipulator. Robotics and Computer-Integrated Manufacturing 2007;23:395–408.
[2] Harib KH, Sharif Ullah AMM, Hammami A. A hexapod-based machine tool with hybrid structure: kinematic analysis and trajectory planning. International Journal of Machine Tools & Manufacture 2007;47:1426–32.
[3] Zhang Y, Liu H, Wu X. Kinematics analysis of a novel parallel manipulator. Mechanism and Machine Theory 2009;44:1648–57.
[4] Rezaei A, Akbarzadeh A, Akbarzadeh-T MR. An investigation on stiffness analysis of a 3-PSP spatial parallel mechanism with flexible moving platform using invariant form. Mechanism and Machine Theory 2012;51:195–216.
[5] Li Y, Xu Q. Kinematics and stiffness analysis for a general 3-PRS spatial parallel mechanism. In: ROMANSY; 2004.
[6] Varedi SM, Daniali HM, Ganji DD. Kinematics of an offset 3-UPU translational parallel manipulator by the homotopy continuation method. Nonlinear Analysis: Real World Applications 2009;10:1767–74.
[7] Ruggiu M. Kinematics analysis of the CUR translational manipulator. Mechanism and Machine Theory 2008;43:1087–98.
[8] Xu Q, Li Y. An investigation on mobility and stiffness of a 3-DOF translational parallel manipulator via screw theory. Robotics and Computer-Integrated Manufacturing 2008;24:402–14.
[9] Clavel R. DELTA, a fast robot with parallel geometry. In: Proceedings of the 18th international symposium on industrial robots; 1988. p. 91–100.
[10] Enferadi J, Akbarzadeh A. A novel spherical parallel manipulator: forward position problem, singularity analysis and isotropy design. Robotica 2009;27:663–76.
[11] Alıcı G, Shirinzadeh B. Loci of singular configurations of a 3-DOF spherical parallel manipulator. Robotics and Autonomous Systems 2004;48:77–91.
[12] Gosselin C, Hamel J. The agile eye: a high-performance three-degree-of-freedom camera-orienting device. In: Proceedings of the IEEE international conference on robotics and automation; 1994. p. 781–6.
[13] Ceccarelli M, Carbone G. A stiffness analysis for CaPaMan (CassinoParallel Manipulator). Mechanism and Machine Theory 2002;37:427–39.
[14] Li Q, Hervé JM. 1T2R parallel mechanisms without parasitic motion. IEEE Transaction on Robotics 2010;26(3):401–10.
[15] Rezaei A, Akbarzadeh A, Enferadi J. Stiffness analysis of a spatial parallel mechanism with flexible moving platform. In: ASME 2010 10th biennial conference on Engineering Systems Design and Analysis, (ESDA2010), vol. 3, Mechanisms and Robotics; 2010. p. 647–55.
[16] Di Gregorio R, Parenti-Castelli V. Position analysis in analytical form of the 3-PSP mechanism. Transactions of the ASME, Journal of Mechanical Design 2001;123:51–7.
[17] Mahmoodi Nia P, Akbarzadeh A. Close form solution for inverse and direct position analysis of a special 3-PSP parallel manipulator. In: 17th international conference on mechanical engineering; 2009.

[18] Kamali K, Akbarzadeh A. A novel method for direct kinematics solution of fully parallel manipulators using basic regions theory. IMechE, Part I: Journal of Systems and Control Engineering 2011;225(5):683–701.
[19] Bonev IA. Geometric analysis of parallel mechanism. PhD thesis. Laval University; 2002.
[20] Liu XJ, Wang J, Pritschow G. Kinematics, singularity and workspace of planar 5R symmetrical parallel mechanisms. Mechanism and Machine Theory 2006;41:145–69.
[21] Altuzarra O, Salgado O, Petuya V, Hernańdez A. Point-based Jacobian formulation for computational kinematics of manipulators. Mechanism and Machine Theory 2006;41:1407–23.
[22] Merlet JP. Jacobian, manipulability, condition number, and accuracy of parallel robots. ASME Journal of Mechanical Design 2006;128:199.
[23] Simaan N, Shoham M. Geometric interpretation of the derivatives of parallel robots' jacobian matrix with application to stiffness control. ASME Journal of Mechanical Design 2003;125:33.
[24] Firmani F, Podhorodeski RP. Singularity analysis of planar parallel manipulators based on forward kinematic solutions. Mechanism and Machine Theory 2009;44(7):1386–399.
[25] Lee TC, Perng MH. Analysis of simplified position and 5-DOF total orientation workspaces of a hexapod mechanism. Mechanism and Machine Theory 2007;42:1577–600.
[26] Tsai KY, Lin JC. Determining the compatible orientation workspace of Stewart–Gough parallel manipulators. Mechanism and Machine Theory 2006;41:1168–84.
[27] Tsai KY, Lee TK, Huang KD. Determining the workspace boundary of 6-DOF parallel manipulators. Robotica 2006;24:605–11.
[28] Rezaei A, Akbarzadeh A. Position and stiffness analysis of a new asymmetric 2PRR-*PPR* parallel CNC machine. Advanced Robotics, http://dx.doi.org/10.1080/0169186 4.2013.751154, in press.
[29] Hao Q, Guan L, Wang J, Wang L. Dynamic feedforward control of a novel 3-PSP 3-DOF parallel manipulator. Chinese Journal of Mechanical Engineering 2011;24(4).
[30] Toutounian F, Saberi-Nadjafi J, Taheri SH. A hybrid of the Newton–GMRES and electromagnetic meta-heurestic methods for solving systems of nonlinear equations. Journal of Mathematical Modelling and Algorithms 2009;8:425–43.
[31] Joshi SA, Tsai LW. Jacobian analysis of limited-DOF parallel manipulators. Transactions of the ASME, Journal of mechanical design 2002;124:254–8.
[32] Zlatanov D, Bonev IA, Gosselin CM. Constraint singularities of parallel mechanisms. In: IEEE International Conference on Robotics and Automation (ICRA 2002); 2002.

Glossary

$B\{x,y,z\}$: The fixed coordinate frame which is attached to point O in top fixed platform;
$T\{u,v,w\}$: The moving coordinate frame which is attached to point T in the center of MS;
a: Distance between the center point O of fixed triangle $\Delta A_1A_2A_3$, and point A_i;
h: Length of the tool;
${}^B\mathbf{a}_i$: The position vectors locate corners of the fixed base, A_i, in frame $\{B\}$.;
${}^B\mathbf{q}_i$: The position vectors which are specified length of each linear rod (LR);
${}^B\mathbf{t}$: The position vector of the end-effector, point T, with respect to $\{B\}$;
${}^B\mathbf{p}$: The position vector of the tool tip, point P, with respect to $\{B\}$;
${}^T\mathbf{h}$: The position vector which connects point T to point P;
${}^B\mathbf{s}_i$: The position vectors of the three spherical joints in frame $\{B\}$;
${}^T\mathbf{b}_i$: The position vectors connect the end-effector to the ith S-joint, S_i in frame $\{T\}$;
${}^B\mathbf{e}_i$: The position vectors connect points A_i to T in frame $\{B\}$;
r: Number of movable rigid bodies (for the 3-PSP parallel robot is equal to 13);
m: Number of one-DOF joints (for the 3-PSP parallel robot is equal to 15);
θ,φ,λ: Rotational variables about the x-, y- and z-axis (Euler angles);
x_T, y_T, z_T: Translational variables of the MS center along the x-, y- and z-axis;
x_P, y_P, z_P: Translational variables for the Tool tip along the x-, y- and z-axis;
q_1, q_2, q_3: Translational variables for the linear rods, LRs;
b_1, b_2, b_3: Translational variables for the MS branches;
${}^B_T\mathbf{R}$: The rotation matrix to transfer a vector defined in $\{T\}$ to $\{B\}$;
$\mathbf{u}$, $\mathbf{v}$, $\mathbf{w}$: Three unit vectors along the u-, v- and w-axis of the moving coordinate frame $\{T\}$;
θ_{mi}: The values for rotational position of motors;
N: Gearbox transmission ratio;
l_b: The lead of the ball screw;
$\mathbf{s}_{normal}$: The normal vector to the MS plane;
$\widehat{\mathbf{s}}_{normal}$: The unit vector along the normal vector to the MS plane, $\mathbf{s}_{normal}$;
$\mathbf{s}_{ij}$: The position vectors which connect the S-joint S_i to the S-joint S_j;
$\{A\}$: The auxiliary coordinate frame, attached to the top fixed platform, at the point A_1;
$\{S\}$: The auxiliary coordinate frame, attached to the moving platform, at the point S_1;
${}^j_i\mathbf{T}$: The transformation matrix which transfers frame $\{i\}$ to frame $\{j\}$;
${}^j_i\mathbf{R}$: A 3×3 rotation matrix which rotates frame $\{i\}$ to frame $\{j\}$;
${}^j_i\mathbf{t}$: A 3×1 vector that locates origin of $\{i\}$ relative to origin of $\{j\}$;
${}^S\mathbf{t}$: The position vector of point T in frame $\{S\}$;
$\dot{\mathbf{q}}$: Vector of the linear actuated joint rates, $[\dot{q}_1 \quad \dot{q}_2 \quad \dot{q}_3]^T$;
$\dot{\mathbf{X}}$: Vector of the MS velocities, $[\mathbf{v}_P \quad \boldsymbol{\omega}_s]^T$;
$\dot{q}_i$: The values of ith actuated joint rate;
$\dot{b}_i$: The values of ith passive prismatic translational joint rate;
v_P: The Cartesian velocity vector for the tool tip, $[\dot{x} \quad \dot{y} \quad \dot{z}]^T$;
$\boldsymbol{\omega_s}$: The angular velocity vector of the MS, $[\dot{\theta} \quad \dot{\varphi} \quad \dot{\lambda}]^T$;
$\widehat{\mathbf{q}}_i$: The unit vectors along ith LRs;
$\widehat{\mathbf{b}}_i$: The unit vectors along ith branch of the MS;
$\widehat{\mathbf{m}}_i$: The three unit vectors which are all perpendicular to the MS plane;
$\widehat{\mathbf{k}}_i$: Unit vectors are perpendicular to planes containing the three vectors, $\mathbf{q}_i$, $\mathbf{e}_i$ and $\mathbf{b}_i$;
$\mathbf{J}_{inv}$, $\mathbf{J}_{dir}$: The inverse and direct Jacobian matrices;
$\mathbf{J}$: The overall Jacobian matrix;
$\mathbf{J}_c$: The Jacobian of constraints;
$\mathbf{J}_{rot}$, $\mathbf{J}_{trans}$: The non-pure rotational and the non-pure translational Jacobian matrices;
$\ddot{\mathbf{q}}$: Vector of the actuated joint linear acceleration, $[\ddot{q}_1 \quad \ddot{q}_2 \quad \ddot{q}_3]^T$;
$\ddot{\mathbf{X}}$: Vector of the MS acceleration, $[\dot{\mathbf{v}}_P \quad \dot{\omega}_s]^T$;
$\ddot{q}_i$: The values of ith actuated joint acceleration;
$\ddot{b}_i$: The values of ith passive prismatic joint linear acceleration;
$\dot{\mathbf{v}}_P$: The Cartesian acceleration vector for the tool tip, $[\ddot{x} \quad \ddot{y} \quad \ddot{z}]^T$;
$\dot{\boldsymbol{\omega}}_{\boldsymbol{s}}$: The angular acceleration vector of the MS, $[\ddot{\theta} \quad \ddot{\varphi} \quad \ddot{\lambda}]^T$.